ML040920189

AN ASSESSMENT OF POSTULATED REACTIVITY-INITIATED ACCIDENTS (RIAs) FOR OPERATING REACTORS IN THE U.S.

1. Background

Hypothetical transients and accidents are used in the design and safety analysis of light-water reactors (LWRs). The postulated events that could challenge the reactor core generally consist of undercooling events (e.g., loss-of-coolant accidents) and overpower events (e.g., reactivity-initiated accidents). The design-basis reactivity-initiated accidents for a pressurized water reactor and boiling water reactor are the control-rod-ejection accident and the control-rod-drop accident, respectively.

General Design Criterion 28 requires that the amount and rate of reactivity increase for RIAs neither damage the reactor coolant pressure boundary nor significantly impair core coolability. A criterion to avoid these consequences is given in Regulatory Guide 1.77 for PWRs, and the criterion is discussed in Section 4.2 of the Standard Review Plan for both PWRs and BWRs. This criterion is a limit of 280 cal/g on the radial average fuel rod enthalpy at the location in the core where this enthalpy is maximum. Lower level criteria exist for the threshold for cladding failure (i.e., a through-wall crack or rupture) to be used in radiological calculations, but those criteria do not generally correspond to limiting conditions.

In 1980, MacDonald et al. reviewed earlier data along with their then-recent data from the Power Burst Facility (PBF).[1] Those data showed that, although some cracks in the cladding could occur at lower fuel enthalpies, the breakup of rods into numerous pieces occurred between about 205 and 240 cal/g. The authors concluded that, if the earlier SPERT and TREAT results had been reported in terms of peak fuel enthalpy instead of deposited energy, a limit of about 230 cal/g might have been chosen instead of 280 cal/g. The NRC staff were well aware of this discrepancy at that time.[2] However, resources were not allocated to correct the regulatory guidance because achievable fuel enthalpies in the event of an RIA were believed to be under 100 cal/g and the change would be inconsequential.

During the 1980s, fuel burnups increased in U.S. power reactors to values well above 40 GWd/t. Research in programs such as the Halden Project in Norway revealed changes in both cladding and fuel pellet behavior around this burnup level. The rate of cladding oxidation increased as a result of developing microcracks in the thick oxide (corrosion) layer, and fuel pellet microstructures changed as large quantities of fission gas accumulated on grain boundaries. It was suspected that these changes might alter the failure behavior of fuel rods under RIA conditions, and tests were planned to investigate this possibility in the Cabri test reactor in France and in the Nuclear Safety Research Reactor (NSRR) in Japan. Similar research was also underway in a Russian program in the Impulse Graphite Reactor (IGR) in Kazakstan, and later tests were performed in the BIGR test reactor in Russia. The Power Burst Facility (PBF) had been shut down by this time, and no such testing was being conducted in the U.S.

In November 1993, test REP-Na1 was run in Cabri and resulted in cladding failure with fuel dispersal at a radial average fuel enthalpy of 30 cal/g.[3] Three months later, test HBO-1 was run in NSRR, and this test also exhibited cladding failure with fuel dispersal at a low enthalpy of

60 cal/g.[4] Much later, REP-Na1 was reexamined because of its unusual characteristics.[5] Nevertheless, many other tests in Cabri and NSRR confirmed the occurrence of low enthalpy failures (below 100 cal/g), often with fuel dispersal.[6]

The Commission was informed of this situation in 1994, and arrangements were quickly made for access to data from the Cabri and NSRR test programs. Arrangements were also made to acquire similar data on tests that had been performed in a Russian program. Later, an NRC program plan for high-burnup fuel was prepared, and criteria and analyses for reactivity accidents were identified for resolution.[7,8] The present paper is intended to provide sufficient information to resolve this issue.

2. Test Data

2.1. SPERT

Early fuel tests under reactivity accident conditions were performed in the SPERT and PBF test reactors in the U.S. The earliest of these tests with irradiated fuel rods were performed during 1969 and 1970 in the SPERT test reactor for the U.S. Atomic Energy Commission. There were several SPERT facilities with different cores, and the core used for the tests of interest was the Capsule Driver Core (CDC), hence these tests are often referred to as CDC tests. Single rods were tested in an instrumented water-filled capsule at ambient conditions. SPERT with the Capsule Driver Core had a natural pulse width of about 20 msec.

Table 1 lists the characteristics of the irradiated fuel tests in the SPERT reactor.[1,9] The test rods were BWR-type fuel rods manufactured to specifications being used by General Electric Co. at that time, except that one group of rods had a smaller outside diameter in order to achieve higher energy depositions. These smaller rods also had a correspondingly reduced cladding thickness. Preirradiation to accumulate the burnup was done in the Engineering Test Reactor (ETR).

Table 1. Characteristics of BWR-type specimens with Zircaloy-2 cladding tested in stagnant water at an initial temperature of 20°C in the SPERT test reactor.*

Test No.	Test Date	Maximum Burnup GWd/t	Oxide Thickness μ	Energy Deposit cal/g	Pulse Width ms	Peak Fuel Enthalpy cal/g	Cladding Strain %	Comments**
CDC-567	1969	3	0	264	18	219		PCMI failure at 214 cal/g No fuel loss
CDC-568	1969	4	0	199	24	165		PCMI failure at <147 cal/g No fuel loss
CDC-569	1969	4	0	348	14	289		PCMI failure at 282 cal/g No fuel loss
CDC-571	1969	5	0	161	31	134		No failure
CDC-684	1970	13	0	200	20	166		No failure
CDC-685	1970	13	0	186	23	154		No failure
CDC-703	1969	1	0	192	15	159		No failure
CDC-709	1969	1	0	238	13	198		PCMI failure at 190 cal/g No fuel loss
CDC-756	1970	32	65	176	17	146		PCMI failure at <143 cal/g No fuel loss
CDC-859	1970	32	65	190	16	158		PCMI failure at 85 cal/g Very little fuel loss

*No entry was made if parameter not measured or not reported in convenient form. Representative value shown if range of values was reported.

2.2. PBF

During the period 1978-1980, reactivity accident tests were performed in the PBF test reactor for the U.S. Nuclear Regulatory Commission. The reactor consists of a driver core in a water pool and a pressurized water test loop that could provide a wide range of test conditions. PBF had a natural pulse width of about 15 msec.

Table 2 lists the characteristics of the fuel tests in the PBF reactor.[10,11,12,13] Tests ST-1 through ST-4 were single-rod tests with fresh PWR-type fuel rods. The remainder of the tests were

performed with PWR fuel rods from the Saxton PWR prototype reactor. Tests RIA 1-1 (rods 801) and RIA 1-2 (rods 802) each contained four fuel rods, but they were in individual flow shrouds such that they behaved as single-rod tests. Test RIA 1-4 (rods 804) was a true multi-rod test with a 3x3 array of nine fuel rods. Test energies were relatively high in the PBF test series because that program was designed to examine fuel behavior near the 280 cal/g fuel enthalpy licensing limit.

Table 2. Characteristics of PWR-type specimens with Zircaloy-4 cladding tested in flowing water at an initial temperature of 265°C in the PBF test reactor.*

Test No.	Test Date	Maximum Burnup GWd/t	Oxide Thickness μ	Energy Deposit cal/g	Pulse Width ms	Peak Fuel Enthalpy cal/g	Cladding Strain %	Comments
RIA 802-1	11/22/78	5	5	240	16	185	3	No failure
RIA 802-2	11/22/78	5	5	240	16	185	6	No failure
RIA 802-3	11/22/78	4	5	240	16	185		PCMI failure at 140 cal/g
RIA 802-4	11/22/78	5	5	240	16	185	5	No failure
RIA ST-1	8/78	0	0	250	22	185		No failure
RIA ST-2	8/78	0	0	345	17	260		
RIA ST-3	8/78	0	0	300	20	225		No failure
RIA ST-4	8/78	0	0	695		350		
RIA 801-1	10/7/78	5	5	365	13	285		Rod fragmented and blocked flow channel during transient
RIA 801-2	10/7/78	5	5	365	13	285		Rod fragmented and blocked flow channel during transient
RIA 801-3	10/7/78	0	0	365	13	285		Rod fragmented and blocked flow channel after transient
RIA 801-5	10/7/78	0	0	365	13	285		Rod fragmented and blocked flow channel during transient
RIA 804-1	4/80	6	5	295	11	277		PCMI failure <<255 cal/g
RIA 804-3	4/80	6	5	295	11	277		PCMI failure <<255 cal/g
RIA 804-4	4/80	5	5	270	11	255		PCMI failure <<255 cal/g
RIA 804-5	4/80	5	5	245	11	234		PCMI failure <<255 cal/g
RIA 804-6	4/80	5	5	270	11	255		PCMI failure <<255 cal/g
RIA 804-7	4/80	6	5	295	11	277		PCMI failure <<255 cal/g
RIA 804-8	4/80	5	5	270	11	255		PCMI failure <<255 cal/g
RIA 804-9	4/80	6	5	295	11	277		PCMI failure <<255 cal/g
RIA 804-10	4/80	5	5	270	11	255		Cladding melted as the result of contact with rods 804-8 and 804-9

*No entry was made if parameter not measured or not reported in convenient form. Representative value shown if range of values was reported.

2.3. CABRI

The first test result with high-burnup fuel that exhibited cladding failure at a low fuel enthalpy came from the CABRI test reactor, which was operated by the Nuclear Safety and Protection Institute in France. The reactor consists of a driver core in a water pool and a test loop with

liquid sodium for the coolant. The test loop was designed for research on fast reactors, but has been used recently to test LWR fuel. Heat transfer in sodium is better than in water, and this is not representative of LWRs. Nevertheless, this facility is capable of energetic pulses, and it can handle highly radioactive high-burnup fuel specimens.

Table 3 lists the important characteristics of the high-burnup fuel tests that have been performed in the CABRI sodium loop.[14,15,16] Although all tests with cladding failure in Cabri exhibit low fuel enthalpies at failure, the first test, REP-Na1, exhibited an extremely low failure enthalpy that has not been seen in other tests. This test has been extensively re-examined, and a final report by an international task force is expected soon.[5] Some investigators, including NRC staff and its contractors, consider this test to be flawed, possibly as the result of preconditioning at an unusually high temperature. Although the results for REP-Na1 are shown below in tables and figures, they are not considered in the conclusions of this report.

Table 3. Characteristics of PWR fuel specimens with Zircaloy-4 cladding (except as noted) tested in flowing sodium at an initial temperature of 280°C in the Cabri test reactor.*

Test No.	Test Date	Maximum Burnup GWd/t	Oxide Thickness μ	Energy Deposit cal/g fuel	Pulse Width ms	Peak Fuel Enthalpy cal/g	Cladding Strain %	Comments
REP-Na1	11/10/93	64	80	111	9.5	114		PCMI failure at 30 cal/g Significant fuel loss
REP-Na2	6/10/94	33	10	207	9.5	199	3.5	No failure
REP-Na3	10/6/94	54	45	122	9.5	124	2.2	No failure
REP-Na4	7/28/95	62	80	95	76	85	0.4	No failure
REP-Na5	5/5/95	64	25	104	8.8	108	1.1	No failure
REP-Na6	3/1/96	47	35	156	32	133	2.6	No failure, MOX**
REP-Na7	1/24/97	55	50	170	40	138		PCMI failure at 113 cal/g, MOX Fuel loss
REP-Na8	7/10/97	60	110	103	75	98		PCMI failure at 78 cal/g No fuel loss
REP-Na9	4/25/97	28	10	233	33	197	7.2	No failure, MOX
REP-Na10	7/30/98	63	80	108	31	98		PCMI failure at 81 cal/g No fuel loss
CIP0-1	11/29/02	75	80	98	32	90		No failure, Zirlo cladding
CIP0-2	11/8/02	77	20	89	28	81		No failure, M5 cladding

*No entry was made if parameter not measured or not reported in convenient form. Representative value shown if range of values was reported.
**Mixed uranium and plutonium dioxide (MOX).

Most of the tests in Cabri have been performed with fuel rods from a commercial PWR in France. Pulse width, which is of special concern and is discussed below, is determined largely by Doppler feedback characteristics of the Cabri core and is relatively fixed. For this test reactor, the natural pulse width is around 9.5 msec. Because this was originally thought to be narrower than a typical PWR prompt-critical pulse, the researchers at CABRI developed a technique to artificially broaden the pulse. Most of the tests in Table 3 were performed with a broadened pulse. Pulse widths are discussed in Section 4.

2.4. NSRR

Tests on medium-to-high-burnup fuel have been underway since 1989 in the NSRR test reactor in Japan, and much of the early work on medium-burnup fuel rods was reported by Fujishiro et al. and Nakamura et al.[17,18] Shortly after the low energy failure occurred in the CABRI program,

failure with fuel dispersal were observed in a high-burnup rod at a low energy in the NSRR test reactor (test number HBO-1). The NSRR reactor is operated by the Japan Atomic Energy Research Institute, and the reactor is a TRIGA-type annular core pulse reactor in a water pool. While a water loop has been used for some testing in NSRR, it is not used with highly radioactive irradiated fuel specimens. Tests with these specimens are conducted in an instrumented capsule at ambient conditions (standard temperature and pressure). The natural pulse width of NSRR depends on the inserted reactivity and is 4.4 ms when the largest pulse is used.

Table 4 lists the important characteristics of high-burnup fuel tests with commercial PWR fuel rods that have been performed in the NSRR test reactor.[19,20,21,22]

Table 4. Characteristics of commercial PWR fuel specimens with Zircaloy-4 cladding (except as noted) tested in stagnant water at an initial temperature of 20°C in the NSRR test reactor.*

Test No.	Test Date	Maximum Burnup GWd/t	Oxide Thickness μ	Energy Deposit cal/g	Pulse Width ms	Peak Fuel Enthalpy cal/g	Cladding Strain %	Comments
MH-1	11/28/89	39	4	63	6.8	47	0.02	No failure
MH-2	3/8/90	39	4	72	5.5	54	0.05	No failure
MH-3	10/31/90	39	4	87	4.5	67	1.56	No failure
GK-1	3/12/91	42	10	121	4.6	93	2.23	No failure
GK-2	3/17/92	42	10	117	4.6	90	1.05	No failure
OI-1	11/10/92	39	15	136	4.4	106	1.49	No failure
OI-2	1/27/93	39	15	139	4.4	108	4.77	No failure
HBO-1	2/16/94	50.4	43	93	4.4	73		PCMI failure at 60 cal Large fuel loss
HBO-2	3/25/94	50	35	51	6.9	37	0.4	No failure
HBO-3	10/19/94	50	23	95	4.4	74	1.5	No failure
HBO-4	1/24/95	50	19	67	5.4	50	0.2	No failure
HBO-5	1/31/96	44	60	102	4.4	80		PCMI failure at 77 cal/g Small fuel loss
HBO-6	2/6/96	49	30	109	4.4	85	1.1	No failure
HBO-7	10/17/96	49	45	112	4.4	88	2.23	No failure
TK-1	11/29/96	38	7	161	4.4	126	25	No failure
TK-2	10/1/97	48	35	136	4.4	107		PCMI failure at 60 cal/g small fuel loss
TK-3	10/8/97	50	10	126	4.4	99	5.6	No failure
TK-4	2/4/98	50	25	125	4.4	98	4	No failure
TK-5	10/1/98	48	30	130	4.4	101	4	No failure
TK-6	10/7/98	38	15	160	4.4	125	15.7	No failure
TK-7	11/20/98	50	30	122	4.4	95		PCMI failure at 86 cal/g No report on fuel loss
TK-8	1/25/00	50	10	84	7	65	0.3	No failure
TK-9	12/25/00	50	<10	126	4.4	99	14.6	No failure
TK-10	2/25/02	46	<10	118	4.4	86		No failure
OI-10	7/11/03	60	27	138	5.6	104	0.72	No failure, MDA cladding
OI-11	7/28/03	58	28	201	4.4	157		PCMI failure at 120 cal/g, Zirlo cladding Fuel fragmentation

*No entry was made if parameter not measured or not reported in convenient form. Representative value shown if range of values was reported.

Table 5 lists the important characteristics of medium-burnup fuel tests with PWR-type fuel rods that were irradiated in the Japan Materials Test Reactor (JMTR) and the Advanced Thermal Reactor (ATR), respectively that have been performed in the NSRR test reactor.

Table 5. Characteristics of PWR-type fuel specimens with Zircaloy-4 cladding that were irradiated in material test reactors and tested in stagnant water at an initial temperature of 20°C in the NSRR test reactor.*

Test No.	Test Date	Maximum Burnup GWd/t	Oxide Thickness μ	Energy Deposit cal/g	Pulse Width ms	Peak Fuel Enthalpy cal/g	Cladding Strain %	Comments
JM-1	7/20/89	22	<2	130	9.3	92	0.1	No failure
JM-2	1/11/90	27	<2	120	9.4	84	0	No failure
JM-3	9/6/90	20	<2	184	8.5	132	0.4	No failure
JM-4	11/6/90	21	<2	235	5.9	177		Failure enthalpy not reported No fuel loss
JM-5	3/5/91	26	<2	220	6.4	167		Failure enthalpy not reported No fuel loss
JM-6	2/13/92	15	<2	212	7.1	156	1	No failure
JM-7	9/9/92	13	<2	201	7.8	146	0.4	No failure
JM-8	9/17/92	20	<2	218	7.2	160	1.6	No failure
JM-9	3/30/93	25	<2	210	6.8	160	0.7	No failure
JM-10	9/27/93	21	<2	270	5.6	200	7.7	No failure
JM-11	12/1/93	31	<2	210	6.3	160	0.9	No failure
JM-12	11/25/93	38	<2	240	5.3	180		Failure enthalpy not reported No fuel loss
JM-13	1/18/95	38	<2	200	6.3	150	0.7	No failure
JM-14	3/7/95	38	<2	210	5.9	160		PCMI failure < 144 cal/g No fuel loss
JM-15	10/11/95	30	<2	200	6.5	150	3.5	No failure
JM-16	10/17/95	38	<2	190	6.4	140	3.2	No failure
JMN-1	11/17/92	22	<2	190	7.1	150		Failure enthalpy not reported No fuel loss
JMH-1	3/23/93	22	<2	200	8.3	150	1.7	No failure
JMH-2	9/30/93	22	<2	250	6.8	180	9.5	No failure
JMH-3	3/13/95	30	<2	270	6.2	220		PCMI failure at 205 cal/g Fuel loss
JMH-4	10/17/96	30	<2	190	7.9	170	3.6	No failure
JMH-5	1/30/97	30	<2	270	6.2	220		PCMI failure at 189 cal/g Fuel loss
ATR-1	3/13/96	20	15	110	6.5	80	0	No failure, MOX
ATR-2	3/14/97	20	15	145	5.1	110	0	No failure, MOX
ATR-3	3/24/97	20	15	155	4.6	120	1.9	No failure, MOX
ATR-4	12/1/97	20	15	180	4.4	140	3.2	No failure, MOX
ATR-5	11/29/99	20	15	180	4.4	140		No failure, MOX
ATR-6	11/8/02	30		110	4.4	85		No failure, MOX

*No entry was made if parameter not measured or not reported in convenient form. Representative value shown if range of values was reported.

Table 6 lists characteristics of medium-burnup and high-burnup fuel tests in NSRR with BWR fuel. These tests were performed with fuel rods from commercial BWRs in Japan.[23]

Table 6. Characteristics of BWR fuel specimens with Zircaloy-2 cladding tested in stagnant water at an initial temperature of 20°C in the NSRR test reactor.*

Test No.	Test Date	Maximum Burnup GWd/t	Oxide Thickness μ	Energy Deposit cal/g	Pulse Width ms	Peak Fuel Enthalpy cal/g	Cladding Strain %	Comments
TS-1	10/24/89	26	6	70	6.0	55	0	No failure
TS-2	2/7/90	26	6	82	5.3	66	0	No failure
TS-3	9/12/90	26	6	109	4.8	88	0	No failure
TS-4	1/17/91	26	6	110	4.6	89	0.4?	No failure
TS-5	1/21/93	26	6	117	4.4	98	0	No failure
FK-1	11/21/96	45	16	167	4.4	130	0.85	No failure
FK-2	2/7/97	45	18	95	6.6	70	0	No failure
FK-3	3/18/98	41	24	186	4.4	145	1.5	No failure
FK-4	1/26/99	56	22	180	4.4	140	1.25	No failure
FK-5	2/19/99	56	22	100	7.3	70	0	No failure
FK-6	3/7/00	61	20 - 30	168	4.4	131		PCMI failure at 70 cal/g Fuel loss
FK-7	3/14/00	61	20 - 30	166	4.4	129		PCMI failure at 62 cal/g No report on fuel loss
FK-8	10/5/00	61	20 - 30	90	7.3	65	0.02	No failure
FK-9	11/1/00	61	20 - 30	119	5.7	90		PCMI failure at 86 cal/g Fuel loss
FK-10	10/12/01	61	20 - 30	135	5.1	103		PCMI failure at 80 cal/g No report on fuel loss
FK-12	12/13/02	61	20 - 30	118	5.8	89		PCMI failure at 72 cal/g No report on fuel loss

*No entry was made if parameter not measured or not reported in convenient form. Representative value shown if range of values was reported.

2.5. IGR

During the 1980s and early 1990s, a large series of reactivity-accident tests was carried out in the IGR test reactor by the Russian Research Center "Kurchatov Institute." The IGR reactor is a uranium-graphite pulse reactor with a central experimental channel. Tests were performed with specimens in capsules under ambient conditions. As a rule, an experimental capsule contained two fuel rods: one high-burnup fuel rod and one fresh fuel rod. For safety reasons, instrument penetrations were not used when irradiated specimens were being tested, so the tests with high-burnup fuel were not instrumented. The natural pulse width for this reactor was about 700 msec, which is much broader than the pulses mentioned above.

Table 7 lists the characteristics of the high-burnup fuel tests in the IGR reactor.[24,25,26] These tests were performed with fuel rods from a commercial VVER in Russia. The main difference between the VVER fuel rods and PWR fuel rods is that the VVER rods have a different cladding alloy and a centerline hole in the fuel pellets.

2.6. BIGR

As recent tests were being conducted in Cabri and NSRR, it was realized that pulse width could have an important impact on test results. Because IGR had such a large pulse width, a new series of tests that were similar to those in IGR were conducted in the BIGR test reactor in Moscow.[27] The BIGR reactor has a very narrow pulse width of about 3 ms, in sharp contrast to

the IGR reactor. Table 8 lists the characteristics of the high-burnup fuel tests in the BIGR reactor.

Table 7. Characteristics of VVER fuel specimens with E110 cladding tested in stagnant water at an initial temperature of 20°C in the IGR test reactor.*

Test No.	Test Date	Maximum Burnup GWd/t	Oxide Thickness μ	Energy Deposit cal/g	Pulse Width ms	Peak Fuel Enthalpy cal/g	Cladding Strain %	Comments
H1T	1990-92	49	5	253	800	151		No failure
H2T	1990-92	48	5	333	760	213		Swelling and rupture; failure time not measured No observation for fuel loss
H3T	1990-92	49	5	384	820	251		Swelling and rupture; failure time not measured No observation for fuel loss
H4T	1990-92	49	5	196	760	114		No failure
H5T	1990-92	49	5	251	840	176		Swelling and rupture; failure time not measured No observation for fuel loss
H6T	1990-92	49	5	141	800	87	0	No failure
H7T	1990-92	47	5	244	630	187		Swelling and rupture; failure time not measured No observation for fuel loss
H8T	1990-92	47	5	109	850	61	0	No failure
H14T	1990-92	0	5	91	900	61	0.5	No failure
H15T	1990-92	0	5	277	900	195		Swelling and rupture; failure time not measured No observation for fuel loss
H16T	1990-92	0	5	195	850	121	0	No failure
H17T	1990-92	0	5	141	950	91	1.5	No failure
H18T	1990-92	0	5	132	850	85	2.4	No failure
H6C	1990-92	0	0	323	800	219		Swelling and rupture; failure time not measured No observation for fuel loss

*No entry was made if parameter not measured or not reported in convenient form. Representative value shown if range of values was reported.

Table 8. Characteristics of VVER fuel specimens with E110 cladding tested in stagnant water at an initial temperature of 20°C in the BIGR test reactor.*

Test No.	Test Date	Maximum Burnup GWd/t	Oxide Thickness μ	Energy Deposit cal/g	Pulse Width ms	Peak Fuel Enthalpy cal/g	Cladding Strain %	Comments
RT-1	1997-00	48	5	174	2.6	142	4	No failure
RT-2	1997-00	48	5	143	2.6	115	1	No failure
RT-3	1997-00	48	5	168	2.6	138	4	No failure
RT-4	1997-00	60	5	152	2.6	125	6	No failure
RT-5	1997-00	49	5	178	2.6	146	5	No failure
RT-6	1997-00	48	5	187	2.6	153	7	No failure
RT-7	1997-00	60	5	165	2.6	134	4	No failure
RT-8	1997-00	60	5	202	2.6	164	11	Swelling and rupture; failure time not measured No fuel loss
RT-9	1997-00	60	5	201	2.6	165	9	Swelling and rupture; failure time not measured No fuel loss
RT-10	1997-00	47	5	207	2.6	164	17	Swelling and rupture; failure time not measured No fuel loss
RT-11	1997-00	47	5	237	2.6	188	8	Swelling and rupture; failure time not measured No fuel loss
RT-12	1997-00	47	5	198	2.6	155	5	No failure

*No entry was made if parameter not measured or not reported in convenient form. Representative value shown if range of values was reported.

2.7. Summary of Data from Test Reactors

Peak fuel enthalpy is the metric for fuel damage during reactivity accidents, and the possible effect of burnup is the reason that the regulatory criteria are being re-examined. Thus, peak fuel enthalpy values for all of the tests mentioned above are shown as a function of burnup in Fig. 1. Open symbols indicate tests without cladding failure, and solid symbols indicate tests with cladding failure. Two things are clear from this plot. First, there is a general downward trend in peak fuel enthalpy for cladding failures as burnup increases. Second, there is a lot of scatter in the data as plotted in this figure.

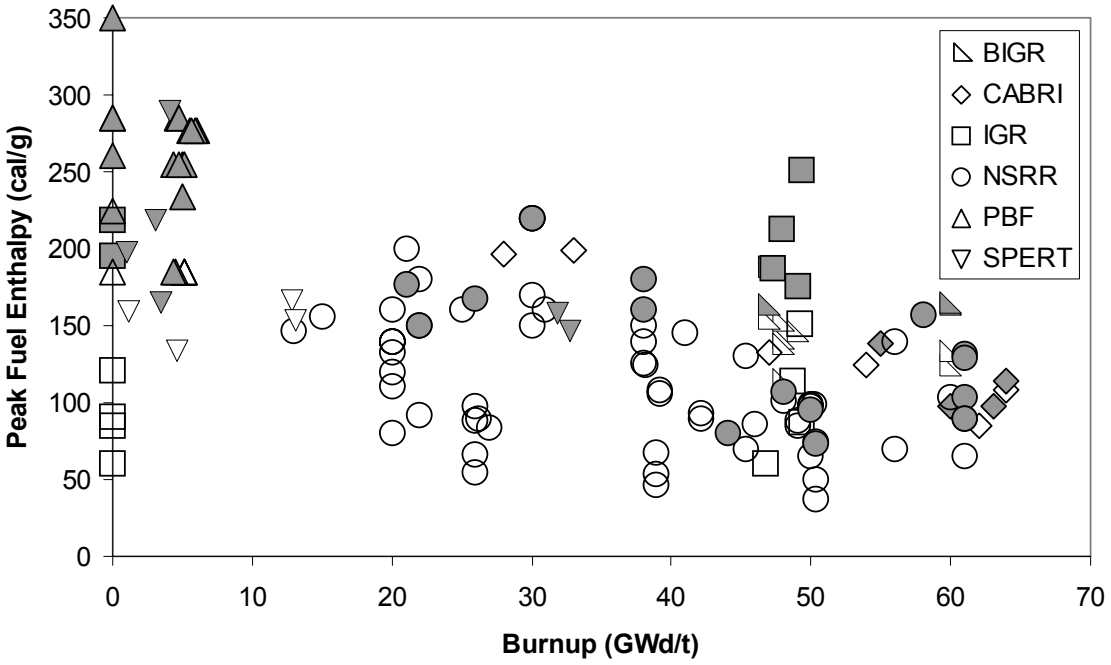

Figure 1. Test data, plotted as peak fuel enthalpy (total) as a function of burnup. Shaded symbols indicate cladding failure.

3. Mechanisms of Cladding Failure and Fuel Dispersal

Early tests in TREAT and SPERT, on which the original 280 cal/g criterion were based, used fuel specimens with low or zero burnup. MacDonald reported that consequences of unirradiated fuel rod failure were insignificant at a radial average peak fuel enthalpy less than about 240 cal/g, whereas prompt fuel dispersal was observed above 275 cal/g.[1] Coolant pressure pulses were also observed at the higher enthalpies. This behavior is consistent with the melting of UO_2. Melting in unirradiated UO_2 begins at 267 cal/g (the solidus temperature), and there is a volumetric expansion of about 10 percent when UO_2 changes from the solid phase to the liquid phase. This sudden expansion leads to cladding failure and prompt fuel dispersal, which in turn causes fuel-coolant interactions (small steam explosions). MacDonald's suggested limit of 230 cal/g would thus guarantee that there would be no fuel dispersal for low-burnup fuel, even if there were cladding failure, and this would ensure the retention of a coolable geometry and the avoidance of a pressure pulse that might damage the pressure boundary.

MacDonald also observed that only previously irradiated rods failed at low energies due to pellet-cladding mechanical interaction (PCMI). This PCMI phenomenon is even more prevalent at high burnups (i.e., greater than about 40 GWd/t). Enhanced corrosion of cladding at high burnup leads to significant hydrogen absorption. For each molecule of water that reacts with zirconium in the corrosion process, about 16% of the hydrogen that is freed is also absorbed in the zirconium.[28] Only about 50 to 100 ppm of hydrogen are soluble in a Zircaloy at 280-330°C, and above these concentrations the excess hydrogen precipitates as zirconium hydride. Concentrations of 200-800 ppm are common in some zirconium alloys at fuel burnups around 60 GWd/t, so most of their hydrogen will be in the form of hydride precipitates. At high burnup, hydride precipitates line up around the circumference and they accumulate near the outside diameter, where the temperature is cooler (see Fig. 2). Zirconium alloys containing high

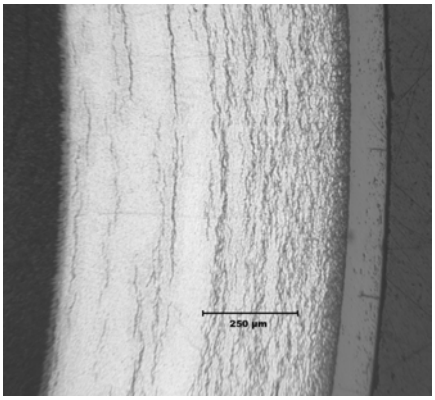

Figure 2. Hydride precipitates in cladding on high-burnup PWR fuel (H. B. Robinson, 67 GWd/t). The outside diameter and oxide layer are on the right.

concentrations of hydride precipitates are more brittle than un-hydrided metal, especially for temperatures below 400°C, and cracks initiate easily. As a consequence, the cladding cannot always deform sufficiently to accommodate the thermal expansion of the fuel pellet, even when fuel melting does not take place, and through-wall cracks develop. Failure by PCMI can occur at fuel enthalpies below 100 cal/g for some commonly experienced corrosion levels.

However, some zirconium alloys with niobium have a lot of ductility and corrosion levels that are so low on high-burnup fuel that cladding failures do not occur by the PCMI mechanism at a low enthalpy level. This was the case for the IGR and BIGR tests with the Russian E110 cladding alloy. Therefore, it is clear that burnup is not the dominant variable with regard to cladding failure during an RIA pulse. Cladding failure is seen to be much more strongly dependent on corrosion (oxidation) than on burnup. Consequently, the data have been re-plotted in terms of fuel enthalpy change as a function of oxide (corrosion) thickness in Fig. 3.

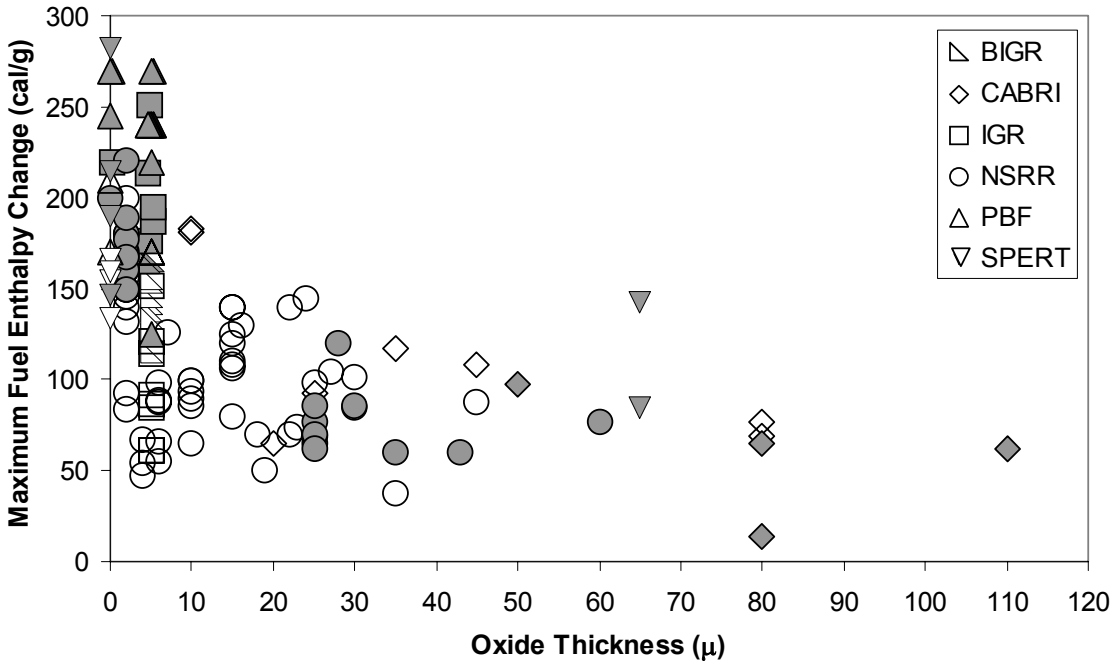

Figure 3. Test data, plotted as maximum fuel enthalpy change as a function of oxide (corrosion) thickness. Shaded symbols indicate cladding failure.

Two additional features of Fig. 3 are significant. First, the stress that the expanding pellet applies to the cladding is more closely related to the change in fuel enthalpy during the test (or an RIA) than to the peak fuel enthalpy, because some stress relaxation will occur during preconditioning at the test temperature. Thus the change in fuel enthalpy has been plotted rather than the total fuel enthalpy. Second, many of these tests were instrumented such that it was possible to tell when the failure occurred and therefore to determine the actual fuel enthalpy change at the time of failure. Thus, the failure points (solid symbols) show the fuel enthalpy change at the time of failure when it is known (see Tables 1-8).

The downward trend of failures is still present, but data scatter in Fig. 3 has been substantially reduced compared with Fig. 1. Some of the remaining scatter is present because test conditions were not the same from test to test, and the most notable differences are in test temperature and pulse width. These test conditions have not only been varied, but they are not always similar to PWR or BWR accident conditions. Variations and atypicalities in pulse width and test temperature are addressed by scaling in Section 5.

Fuel microstructure also changes with burnup, and microstructure affects fuel dispersal. Prompt heating of fission gas bubbles that accumulate at high burnup on grain boundaries can explode the grain structure, driving fuel particles into the coolant under certain conditions. One pre-condition, obviously, is that the cladding must have ruptured or split for the fuel particles to exit. Several other pre-conditions may be necessary: (a) rapid heating, such that the high-pressure gas bubbles cannot depressurize benignly by expansion or venting of their gas into the large effective fuel rod plenum volume, (b) excess enthalpy above that required for failure, and (c) sufficient burnup to create a large accumulation of fission gas bubbles on grain boundaries. Table 9 summarizes the failure data for high-burnup fuel and shows when fuel dispersal occurred in relation to these factors.

Some conclusions can probably be reached from these data. Generally, more fuel dispersal is seen with narrow pulses than with broad pulses. However, there are noticeable exceptions. For example, even with the narrow pulse in the BIGR tests (2.6 ms), the failure was delayed while the cladding heated up during swelling and rupture. Hence, the failure did not occur until after the gas bubble expansion had taken place and fuel was not expelled. Many of the NSRR JM series tests with narrow pulses (5.3-7.1 ms) did not disperse fuel, but these rods were all irradiated in a test reactor rather than a commercial reactor and may have behaved differently for some reason. The Cabri test, REP-Na7, had a broad pulse (40 ms), but still dispersed fuel; however, this was a MOX fuel and might have behaved differently from UO_2 fuel with regard to dispersal.

We will not rely on any conclusions about a relation between pulse width and dispersal in this assessment. We will simply recognize that expanding fission gas bubbles can disperse fuel particles from high-burnup fuel during an RIA pulse, whereas molten fuel expansion was required to disperse fuel particles from low-burnup fuel.

Table 9. Summary of fuel dispersal observations for tests with high-burnup fuel.

Test		Pulse Width ms	Maximum Burnup GWd/t	Failure Enthalpy cal/g	Peak Fuel Enthalpy cal/g	Dispersal Yes or No
BIGR	RT-8	2.6	60	N/A	164	No
	RT-9	2.6	60	N/A	165	No
	RT-10	2.6	47	N/A	164	No
	RT-11	2.6	47	N/A	188	No
NSRR	HBO-1	4.4	50	60	73	Yes
	HBO-5	4.4	44	77	80	Yes
	TK-2	4.4	48	60	107	Yes
	OI-11	4.4	58	120	157	Yes
	JM-4	5.9	21	N/A	177	No
	JM-5	6.4	26	N/A	167	No
	JM-12	5.3	38	N/A	180	No
	JM-14	5.9	38	<144	160	Marginal
	JMN-1	7.1	22	N/A	150	No
	JMH-3	6.2	30	205	220	Yes
	JMH-5	6.2	30	189	220	Yes
	FK-6	4.4	61	70	131	Yes
	FK-9	5.7	61	86	90	Yes
Cabri	REP-Na1	9.5	64	30	114	Yes
	REP-Na7	40	55	113	138	Yes
	REP Na-8	75	60	78	98	No
	REP-Na10	31	63	81	98	No
Spert	CDC-859	16	32	85	158	Marginal
	CDC-756	17	32	<143	146	No

4. Pulse Widths

During a postulated rod-ejection accident in a PWR, the rate of reactivity insertion would be high enough for the reactor to go prompt critical. The resulting linear power may be many times higher than during normal operation, and the shape of the power pulse is determined by the reactivity inserted, Doppler feedback, and other factors. Two typical PWR pulses for a postulated rod-ejection accident are shown in Fig. 4.

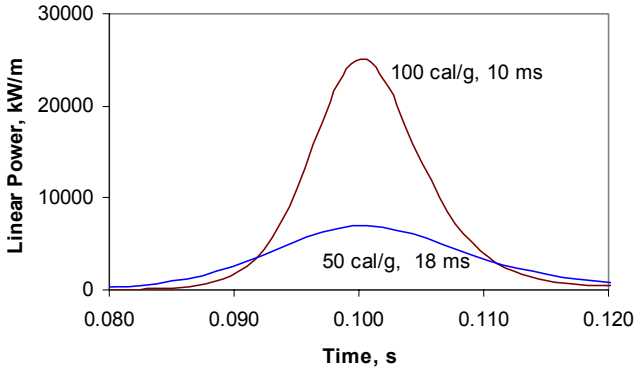

Figure 4. Two PWR pulses of different energy and pulse shape.

An inverse relation exists between pulse height and pulse width, and this relation is given analytically in an ideal case by the Nordheim-Fuchs equation.[29] We have explored this relation for several real reactor cases, and we have examined calculations performed by others.[30] From these calculations, it is found that pulse width (full width at half maximum, FWHM) as a function of the change in fuel enthalpy during a transient varies as shown in Fig. 5.

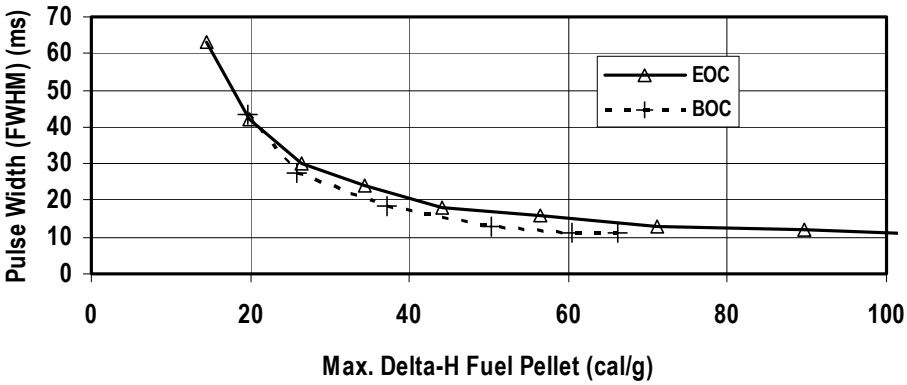

Figure 5. Dependence of pulse width on energy (fuel enthalpy change) for beginning of cycle (BOC) and end of cycle (EOC) conditions.

The main consequence of this relation is that narrow pulses are more adiabatic than broad pulses, and this will affect cladding temperature. The effect of pulse width on cladding temperature can be seen in Fig. 6. This figure shows average cladding temperature as a

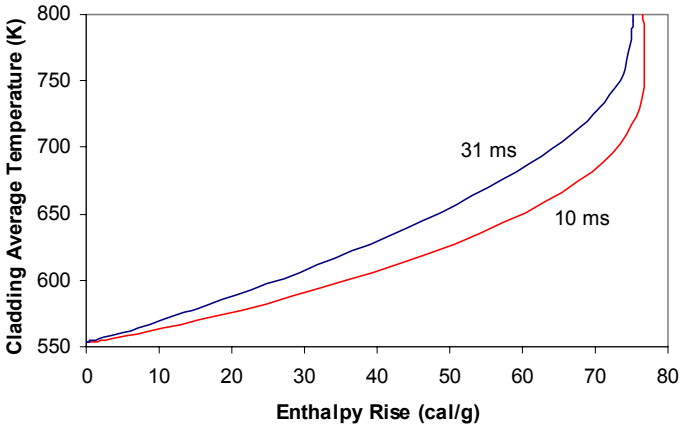

Figure 6. Average cladding temperature as a function of fuel enthalpy change

function of the change in fuel enthalpy. The change in fuel enthalpy can be considered approximately equivalent to fuel pellet expansion, which is the source of both stress and strain that challenge the cladding. As the change in fuel enthalpy increases toward its maximum value, a given enthalpy change produces a higher cladding temperature with a broader pulse. Thus, a given cladding stress or strain occurs at a higher cladding temperature with a broader pulse. For the broader pulse, the higher cladding temperature may, in turn, reduce the tendency for cladding failure.

During a postulated rod-drop accident in a BWR, the rate of reactivity insertion is slower than in a PWR because of velocity limiters on each control blade. For this and other reasons, RIA pulses in a BWR are generally broader than in a PWR.

5. Scaling Method

5.1 Outline of Method

Most of the test data for fuel with corrosion levels of interest have been obtained with PWR fuel rods in the Cabri test reactor in France and the Nuclear Safety Research Reactor (NSRR) in Japan. However, neither of these facilities reproduces conditions in a commercial reactor, so it is desirable to scale these data to PWR conditions to obtain relevant results.

There are several ways to use test reactor data for RIA analysis for commercial reactors. One way is to use the data to validate a transient fuel rod code and then perform the commercial reactor analysis with that code. The difficulty with this use of test reactor data is that it assumes that an appropriate failure model is available in the code and that all code modeling assumptions and materials properties data are adequate for RIA analysis. Modeling assumptions (e.g., symmetric fuel pellet loading of the cladding, homogeneous and isotropic cladding mechanical properties) are not very accurate, and the mechanical properties data base for irradiated cladding is quite limited at this time. But the biggest difficulty is with the failure model; a broadly accepted understanding of RIA failures is not yet available. In fact, the failure modes observed to date range from brittle to mixed to ductile. Also, the presence of non-homogeneous hydride precipitates and blisters may have a significant impact on the failure mode.

To minimize these uncertainties, a more direct way of using test reactor data has been chosen. For a test with cladding failure, this method takes code predictions of stress and strain at the reported time of cladding failure to be the failure stress and failure strain for the fuel rod segment used in the test. In order to predict failure of this fuel rod segment in a PWR environment, it is first necessary to estimate how those failure stress and strain values would change for different conditions – principally temperature – and then run the calculation again for PWR conditions.

Three tests in Cabri resulted in cladding failure, and those tests are analyzed. In addition, two tests with cladding failure in different NSRR test series are analyzed. Analysis of these five test results – together with the data in Fig. 3 – provide enough information to estimate the failure threshold for cladding under PWR conditions.

In the paragraphs that follow, reference is made to elastic and plastic properties of the cladding. The terms that are used are defined in Fig. 7 in relation to a typical stress-versus-strain plot.

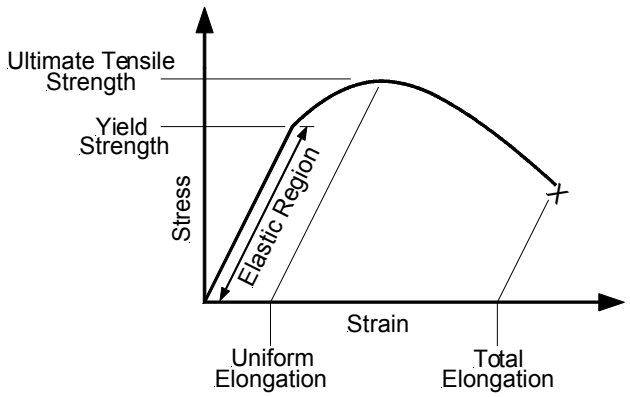

Figure 7. Terms used to describe elastic and plastic properties of cladding.

5.2. Variation of Failure Stress with Temperature

For failures that occur in or near the elastic region, cladding hoop stress is the most important parameter. Failure is assumed to occur with little or no plastic deformation (i.e., no measurable change in cladding diameter) and at a specific stress (failure stress), which is a function of the fracture toughness, flaw size, and a geometric constant representative of the configuration of the cracked structure. However, for scaling purposes, the flaw size, distribution of flaws, and thus the geometric constant are assumed to be identical for a given specimen under test reactor and commercial reactor conditions.

Figure 8 shows fracture toughness of Zircaloy-4 containing 400-1300 ppm hydrogen as a function of temperature.[31] The temperature dependence is small at lower temperatures, but by 250°C the fracture toughness starts increasing rapidly.

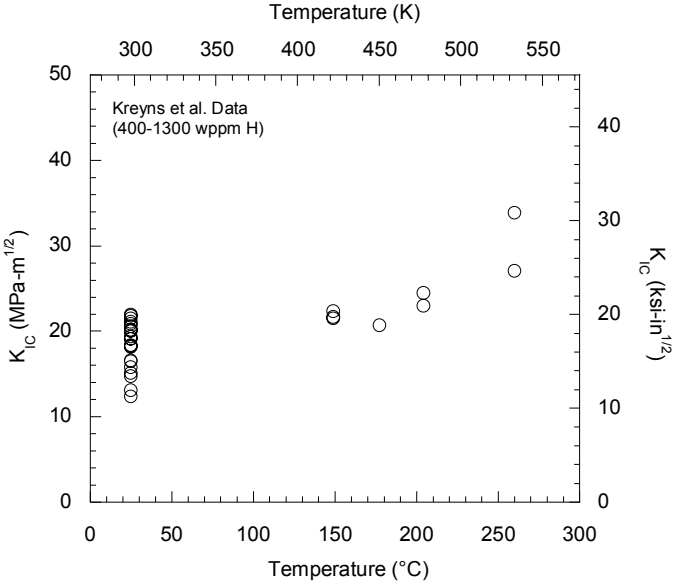

Figure 8. Fracture toughness of Zircaloy as a function of temperature.

Other data also show this trend.[32] Although the exact temperature of this large increase may vary with hydrogen content and other parameters, the trend depicts a transition from brittle to ductile failure somewhere around 300°C.

Scaling of test data using hoop stress as the key parameter will be performed for the Cabri test, REP-Na10. The cladding in this test failed with little or no change in cladding diameter. Microscopically, the fracture surface reveals fracture propagation via localized brittle failure of densely distributed hydrides mixed with plastically deformed metal, resulting in a saw-tooth-like crack line. Nevertheless, the crack tip is perpendicular to the cladding surface, indicating very little plastic strain (see Fig. 9).[a]

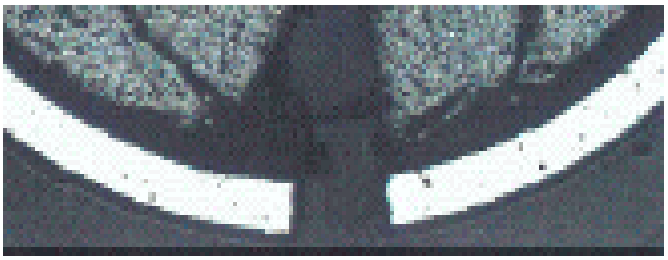

Figure 9. Cross section of REP-Na10 fuel rod shows a crack tip that is perpendicular to the cladding surface and indicates little or no plastic strain.

This test, REP-Na10, like all tests in Cabri, was conducted with an initial uniform temperature of 280°C, which corresponds to the hot zero-power temperature in a PWR. The average cladding temperature increased almost 200 degrees by the time of reported cladding failure, according to our calculations. By this time, the cladding average temperature was well above the brittle-to-ductile transition temperature, yet macroscopically ductile failure (i.e., significant diameter change) was not observed.[b] The implication is that temperature-related processes that alter the fracture toughness were not able to operate sufficiently during the short time of the pulse (31 ms FWHM) to make the cladding ductile. Therefore, in the analysis that follows, it is assumed that fracture toughness is frozen at the initial test temperature and does not vary during the pulse.

5.3. Variation of Failure Strain with Temperature

For failures that occur with substantial plastic hoop strain, ductility is the most important parameter. Figure 10 is a cross section of NSRR's HBO-1 test rod after failure, showing the

---

[a]A large crack in the fuel pellet is seen adjacent to the cladding failure. This crack might have affected cladding failure in some way, but we do not have any analytical means of accounting for the crack. No similar pellet cracks were seen at failure locations in other test cases that we analyzed.

[b]Cladding average temperature here and elsewhere in the report means the wall-averaged temperature at the peak power location.

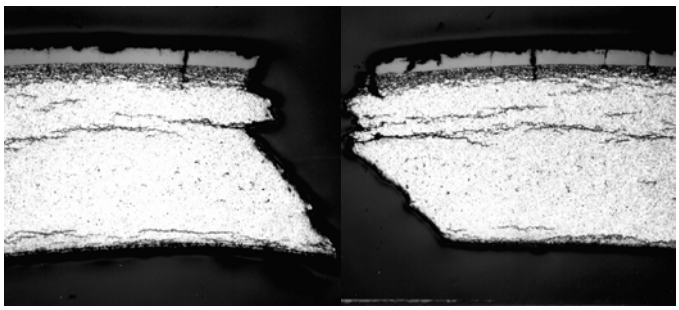

Figure 10. Cross section of HBO-1 fuel rod showing 45-degree crack tip that indicates significant plastic strain.

characteristic 45-degree shear failure that is indicative of significant plastic strain. This crack tip appearance is typical of most of the test results from NSRR. For these types of cladding failures, strength may no longer be significant as a failure limit because cladding deformation can progress beyond yielding (yield stress) – and beyond uniform elongation (ultimate tensile strength) in some cases. Failure can occur by propagation of a mixed-mode crack or by local plastic instability (necking), in which case the failure strain would be a total elongation, although this would not be directly related to total elongation measured in uniaxial tensile tests.

Neither the uniform elongation nor the total elongation for failure under RIA conditions is well characterized by tensile test data. In particular, total strain measured in these tests is highly dependent on test specimen geometry and loading method, and these cannot be made exactly like the loading under RIA conditions. Nevertheless, it will be assumed that the temperature dependence observed in such tests is applicable to plasticity under RIA conditions.

Localized plasticity is not usually modeled in codes such as FRAPTRAN, which can only model uniform plasticity.[33] Therefore, it is not clear whether calculated failure strain should be related to uniform elongation or to total elongation for purposes of temperature dependence, so both are used in the following analysis to see the range of results.

Figure 11 shows uniform elongation as a function of temperature based on PROMETRA data from France.[34] These data come from uniaxial tests in the hoop direction on irradiated Zircaloy cladding. Although uniaxial tests do not produce the appropriate strain path for RIA conditions, the temperature dependence should be similar for all strain paths. Other data show similar trends.[35] For temperatures up to about 400°C, no clear temperature dependence is seen, as indicated by the horizontal line. Above about 400°C, an increase in uniform elongation with increasing temperature is seen, as would be expected because these temperatures are most likely above the irradiation temperature (resulting in annealing of radiation-induced defects) and above the brittle-to-ductile transition temperature for hydrides.

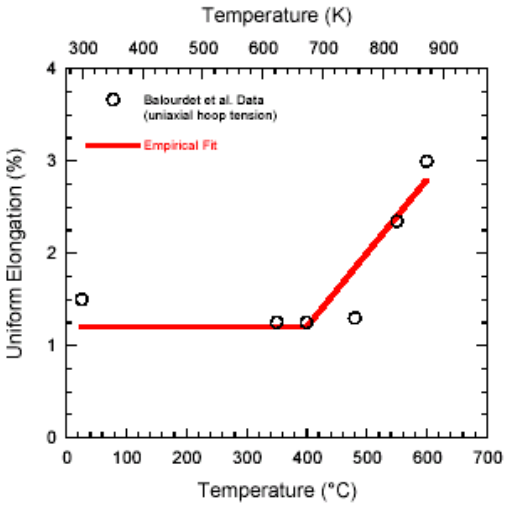

Figure 11. Uniform elongation of irradiated Zircaloy as a function of temperature.

Figure 12 shows total elongation as a function of temperature from the same PROMETRA program. Other data also show a similar trend, which is represented by a simple linear fit.

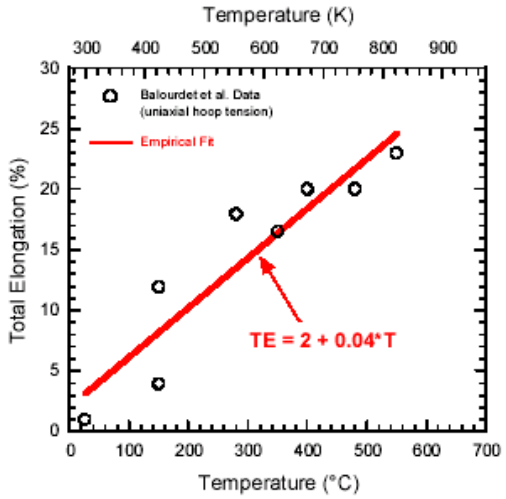

Figure 12. Total elongation of irradiated Zircaloy as a function of temperature.

Plastic deformation involves lattice defects (including radiation-induced defects), and the concentration of these defects can be temperature dependent. However, to change the concentration requires some atomic migration (diffusion), which takes time. The need for some elapsed time would show up in tests as a heating rate effect, and there are data that show such a reduction in temperature dependence with increasing heating rate.[36] Therefore, for the very rapid heating that occurs during RIA pulses, the assumption is made that the plastic properties are frozen at the initial test temperature and do not vary during the pulse — just as was assumed for fracture toughness.

With this assumption, the temperature dependence of the plastic properties only comes into play for the NSRR specimens, which were tested at room temperature rather than at hot reactor temperature of about 280°C. Hence scaling will be done to account for this temperature difference. Because these temperatures are below 400°C, there will be no temperature adjustment for the cases in which uniform elongation is used.

5.4. Variation of Elastic Properties with Temperature

Young's modulus and yield points are built into the FRAPTRAN code and they change with temperature. Figure 13 shows the values in FRAPTRAN for two different temperatures. Notice

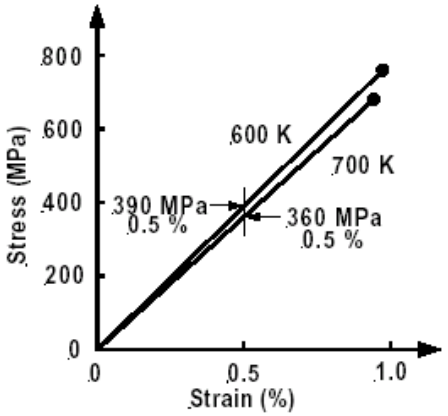

Figure 13. Stress versus strain in the elastic region from the elastic modulus in FRAPTRAN at two different temperatures.

that for any given strain value, the stress is higher at the lower temperature. If strain is related to fuel enthalpy, this shows in general that higher stresses are generated at lower temperatures for the same fuel enthalpy. Conversely, yielding always occurs at a smaller strain value (i.e., limit strain) at higher temperatures.

Whereas the plastic properties discussed in Sections 5.2 and 5.3 involve the movement of lattice defects and require time to change, the elastic properties are determined by interatomic forces acting in a perfect lattice and will respond instantaneously. Consequently, in FRAPTRAN the elastic properties change with temperature during the RIA pulses and affect the results even though we have assumed that plasticity and toughness do not change during the pulses.

5.5. Strain Data and Calculations

Measured plastic hoop strains for tests with non-failed cladding in Cabri and NSRR are shown in Fig. 14. Strain was not measured for tests with cladding failure. Strains above 3%, which were observed at high energies in some tests, have been omitted from this figure because those large strains are the result of high-temperature swelling rather than PCMI and are not of interest here. The apparent zero-strain intercept in Fig. 14 corresponds to the enthalpy required to close the gap and to expand the cladding through the elastic range; only then does

permanent plastic deformation begin.

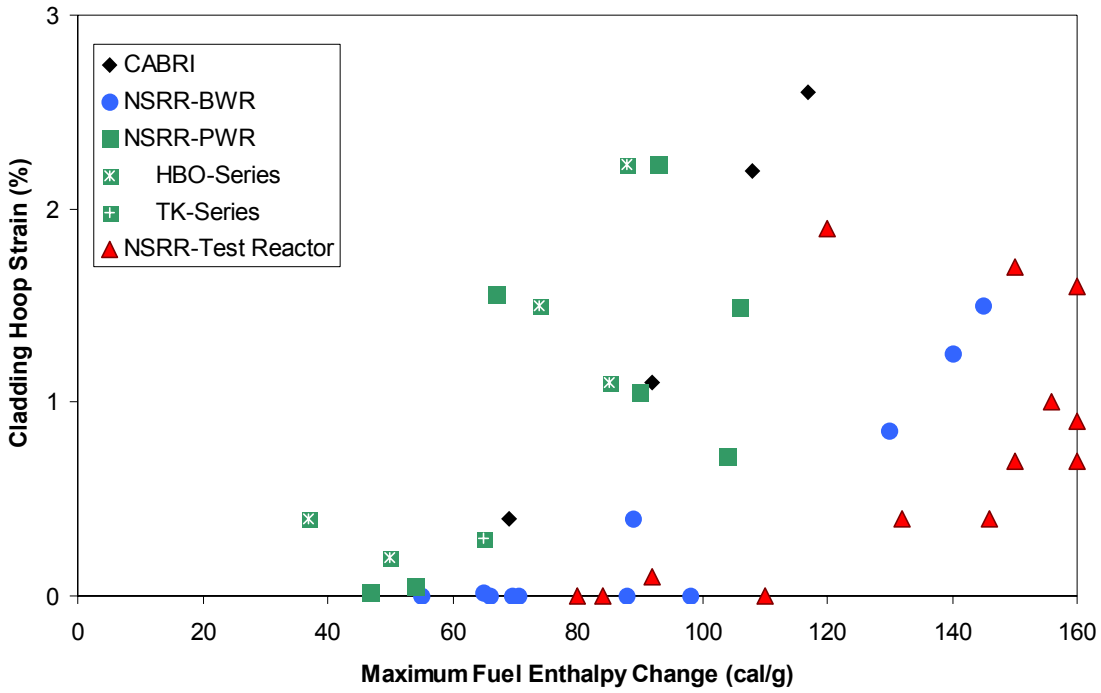

Figure 14. Plastic strain measured from non-failed cladding as a function of maximum fuel enthalpy change for tests in Cabri and NSRR.

There is a very large spread in apparent zero-strain intercept values in Fig. 14, ranging from 25 to more than 100 cal/g. The strain data from NSRR tests appear to be segregated, with data from the PWR rods on the left, data from the BWR rods in the center, and data from rods irradiated in the JMTR and ATR materials test reactors on the right. This major grouping is believed to result from significant differences in end-of-life gap size. Hard gap closure occurs in PWR rods that have relatively thin cladding and are irradiated in a high pressure environment. BWRs and low-pressure test reactors produce much less gap closure by creepdown than PWRs for a given burnup. Hence, the onset of plastic strain is delayed in the BWR rods and the rods that received their base irradiation in test reactors.

If attention is focused on the data from PWR rods, there is still significant scatter in the NSRR data, and the NSRR data are generally to the left of the Cabri data. This relative displacement is contrary to initial expectations. Because the NSRR tests were all performed from around room temperature and the Cabri tests were all performed from 280°C, one would expect the PWR rods in NSRR to have larger initial gaps than the rods in Cabri. This would delay the onset of plastic strain more in the NSRR rods than in the Cabri rods, but the opposite is observed.

Pulse width is probably not the explanation. The Cabri tests used a wide range of pulse widths (9-75 ms) and show very little scatter in the strain data. Two recent Cabri tests (CIP0-1 and CIP0-2) also correlate well with the Cabri data shown, but the strain data for these tests have

not been released and therefore are not plotted in the figure. The NSRR tests, on the other hand, were all conducted with about the same pulse width (~5 ms), yet those tests resulted in significant scatter in the strain data.

One possible explanation for this behavior is related to fuel chips and fines (see Fig. 15). After quiescently cooling down from its last power level in an LWR, the fuel rod's gap will open and look something like Fig. 15(a). The gap, as shown, is probably distributed among pellet cracks as well as any open space between the pellet surface and the cladding inside surface. During specimen preparation at room temperature, it is likely that chips and fines get into the open cold gap (see Fig. 15(b)) causing lockup. This stochastic process could lead to a wide variation in

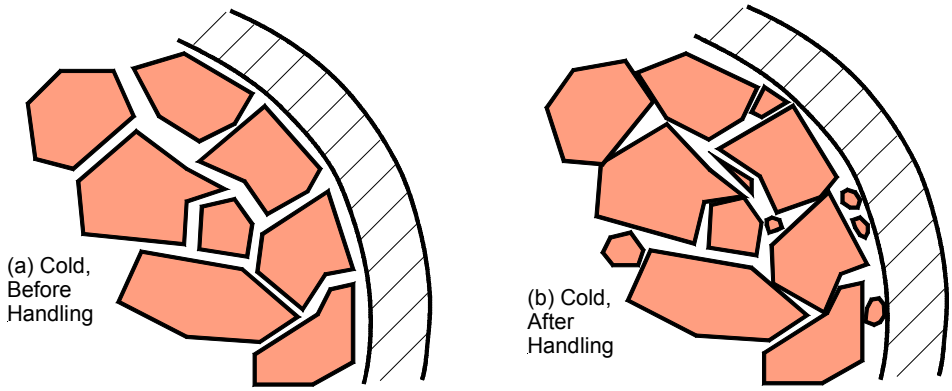

Figure 15. Open gap (actually, distributed cracks) after cooldown from power, (a) before handling and (b) after handling and specimen preparation.

effective cold gap size with regard to the stress that is applied to the cladding. The same process would take place for Cabri tests, but those specimens are held at a high temperature for a long time prior to testing. This preconditioning might compress or relocate the fuel chips and fines, leading to a more well defined effective gap. Hence, the rods tested in Cabri (all PWR rods) could have a larger effective gap than the PWR rods tested in NSRR, and this would lead to a bigger delay in the onset of plastic strain in Cabri than in NSRR, as observed.

No models are present in FRAPTRAN to account for this wide scatter in the observed strain values. Consequently, it was necessary to adjust the input cold gap size to match the particular test series that was being analyzed. For the Cabri tests, the most critical analysis turned out to be for REP-Na10. For that test, there is the observation of a blunt crack tip (discussion below), which indicates that there was little or no plastic strain at the time of failure. A cold gap of 95 microns in the FRAPTRAN analysis was the smallest gap size that would produce strains still within the elastic region at the time of failure for REP-Na10. Larger gap sizes, of course, would also do that, but larger gaps produced results that began to deviate from the Cabri data plotted in Fig. 14. All other cases with initial temperatures around 280°C were also analyzed with this input gap size.

A much smaller value of input gap was used for the NSRR test pulses. Because there is so much scatter in the NSRR data, the choice of input gap size for NSRR tests was more uncertain. A value of 10 microns was selected because it fits data for the HBO series better than a larger gap.

6. Scaling Results

6.1. Cabri REP-Na10 (failure in the elastic region)

Measured test parameters for REP-Na10 are shown in Table 10.

Table 10 Measured Parameters for REP-Na10	
Initial Coolant Temperature	280°C
Total Energy Deposited	108 cal/g
Pulse Width (Full Width at Half Maximum, FWHM)	31 ms
Time of Peak Power	0.446 s
Time of Failure	0.456 s

As discussed above in Section 5.2, this test was analyzed by examining the failure stress in the elastic region. Using FRAPTRAN, hoop stress and other parameters were calculated as a function of time for the actual test reactor pulse. Calculated parameters at the reported time of failure for REP-Na10 are shown in Table 11.

Table 11 Calculated Parameters for REP-Na10	
Effective Gap (Input)	95 μ
Cladding Hoop Stress = Failure Stress	230 MPa
Cladding Average Temperature	525°C
Fuel Enthalpy Change at Failure	59 cal/g

Notice that the calculated fuel enthalpy change at the time of failure (59 cal/g) is in good agreement with the zero-strain intercept of measured strain data in other Cabri tests, as shown in Fig. 14. The calculated value of fuel enthalpy change is also in good agreement with the value reported by the French investigators (65 cal/g; see Table 3 and subtract 16 cal/g from their calculated enthalpy at failure to correct for the initial test temperature).

A second calculation was run with the same deposited energy, but with a pulse shape and other input corresponding to PWR conditions. Power traces for the REP-Na10 test pulse and the PWR-shaped pulse with the same deposited energy are shown in Fig. 16. Using the method described in Sections 5.1 and 5.2, cladding failure should occur for this specimen when the calculated hoop stress in the second calculation reaches 230 MPa; no change in fracture toughness or failure stress was made because the Cabri test was run at the pre-transient PWR temperature. This hoop stress occurs at 46 cal/g enthalpy change in the second calculation. Notice that the calculation indicates a 13 cal/g decrease in enthalpy at failure (59 - 46 = 13). This decrease results from the fact that the stresses developed in the cladding are higher at the lower temperatures (lower enthalpies) in the narrower pulse than at the higher temperatures in the broader pulse (see Section 5.4 above).

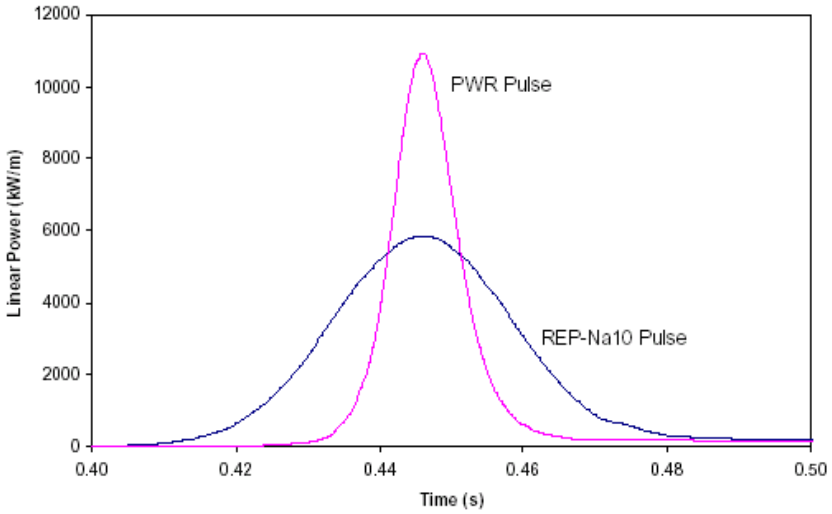

Figure 16. Power versus time for the broad REP-Na10 test pulse and a PWR-shaped pulse with the same deposited energy.

However, higher stress values were calculated at later times in the second calculation. Because we are ultimately interested in a cladding failure threshold, a pulse is desired that has the minimum deposited energy that will result in a peak hoop stress of 230 MPa. The energy deposited in this second calculation is obviously too high.

Additional calculations were performed to search for the smallest pulse that would reach 230 MPa cladding hoop stress. The results for this threshold pulse are given in Table 12.

Table 12 Calculated Parameters for a Threshold Pulse with the REP-Na10 Specimen under PWR Conditions

Inlet Coolant Temperature (Input)	280°C
Total Energy Deposited (Input)	85 cal/g
Pulse Width (FWHM, Input)	13 ms
Effective Gap (Input)	95 μ
Peak Cladding Hoop Stress = Failure Stress	230 MPa
Cladding Average Temperature at Failure	500°C
Maximum Fuel Enthalpy Change	57 cal/g

This calculation has produced a different result. The peak fuel enthalpy that will generate the failure stress of 230 MPa is only 2 cal/g lower than the failure enthalpy observed in the test, rather than 13 cal/g lower as found in the second calculation. Part of this difference (4 cal/g) is the result of using the peak fuel enthalpy instead of the enthalpy at the time of failure. Part of this difference (7 cal/g) is due to rate effects. Near the end of the pulse, when the peak stress is developed, the rate of fuel enthalpy change is approaching zero. At that time, however, the

cladding temperature is still increasing at a rapid rate. Thus it takes more enthalpy to produce a given stress near the end of the pulse than earlier.

6.2. Cabri REP-Na8 (transition from elastic to plastic region)

Measured test parameters for REP-Na8 are shown in Table 13. Pulse width control did not

Table 13 Measured Parameters for REP-Na8	
Initial Coolant Temperature	280°C
Total Energy Deposited	103 cal/g
Pulse Width (Full Width at Half Maximum, FWHM)	75 ms
Time of Peak Power	0.48 & 0.53s
Time of Failure	0.532 s

work as intended in this test, and a very broad double-peaked curve resulted. Power traces for the REP-Na8 test pulse and the corresponding PWR-shaped pulse with the same deposited energy are shown in Fig. 17. Most crack tips for this test are similar in appearance to that

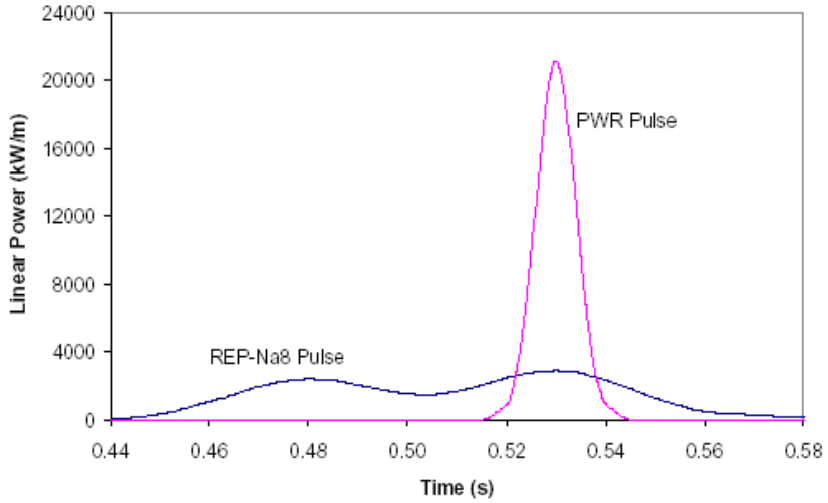

Figure 17. Power versus time for the broad REP-Na8 test pulse and a PWR-shaped pulse with the same deposited energy.

shown in Fig. 9, and little plastic deformation was expected (no reliable measurements were possible because of the interaction between sodium and UO_2).

Our analysis predicted no plastic deformation by the reported time of cladding failure (in the calculation, plastic deformation was initiated less than 2 ms after the reported time of failure), although this could easily be affected by uncertainties in the initial gap size that was assumed

and the measurement of the time of failure. Thus, this test was also analyzed by examining the failure stress, and the method should work even for small plastic strain values that occur before reaching the peak hoop stress. Using FRAPTRAN, hoop stress and other parameters were calculated as a function of time for the actual test reactor pulse. Calculated parameters at the reported time of failure for REP-Na8 are shown in Table 14.

Table 14 Calculated Parameters for REP-Na8	
Effective Gap (Input)	95 μ
Cladding Hoop Stress = Failure Stress	130 MPa
Cladding Average Temperature	560°C
Fuel Enthalpy Change at Failure	63 cal/g

The calculated fuel enthalpy change at the time of failure for REP-Na8 (63 cal/g) is in good agreement with the zero-strain intercept of measured strain data in other Cabri tests, as shown in Fig. 14. The calculated value of fuel enthalpy change is also in good agreement with the value reported by the French investigators (62 cal/g; see Table 3 and subtract 16 cal/g from their calculated enthalpy at failure to correct for the initial test temperature).

A second calculation was run with the same 103 cal/g deposited energy, but with a pulse shape and other input corresponding to PWR conditions. Using the method described in Sections 5.1 and 5.2, cladding failure should occur for this specimen when the calculated hoop stress in the second calculation reaches 130 MPa; no change in fracture toughness or failure stress was made because the Cabri test was run at the pre-transient PWR temperature. This hoop stress occurs at 39 cal/g in the second calculation. Notice that the calculation indicates a 24 cal/g decrease in enthalpy at failure (63 - 39 = 24). This decrease results from the fact that the stresses developed in the cladding are higher at the lower temperatures (lower enthalpies) in the narrower pulse than at the higher temperatures in the broader pulse (see Section 5.4 above).

As with REP-Na10, however, higher stress values were calculated at later times in the second calculation. Because we are ultimately interested in a cladding failure threshold, a pulse is desired that has the minimum deposited energy that will result in a peak hoop stress of 130 MPa. The energy deposited in this second calculation is obviously too high.

Additional calculations were performed to search for the smallest pulse that would reach 130 MPa cladding hoop stress. The results for this threshold pulse are given in Table 15. This calculation has produced a different result. The peak fuel enthalpy that will generate the failure stress of 230 MPa is only 9 cal/g lower than the failure enthalpy observed in the test, rather than 24 cal/g lower as found in the second calculation. Part of this difference (4 cal/g) is the result of using the peak fuel enthalpy instead of the enthalpy at the time of failure, and part (11 cal/g) is due to rate effects as discussed for REP-Na10.

Table 15 Calculated Parameters for a Threshold Pulse with the REP-Na8 Specimen under PWR Conditions	
Inlet Coolant Temperature (Input)	280°C
Total Energy Deposited (Input)	65 cal/g
Pulse Width (FWHM, Input)	16 ms
Effective Gap (Input)	95 μ
Peak Cladding Hoop Stress = Failure Stress	130 MPa
Cladding Average Temperature at Failure	500°C
Maximum Fuel Enthalpy Change	54 cal/g

6.3. Cabri REP-Na7 (failure in the plastic region)

Measured test parameters for REP-Na7 are shown in Table 16. The fuel rod for REP-Na7

Table 16 Measured Parameters for REP-Na7	
Initial Coolant Temperature	280°C
Total Energy Deposited	172 cal/g
Pulse Width (Full Width at Half Maximum, FWHM)	40 ms
Time of Peak Power	0.405 s
Time of Failure	0.452 s

contained MOX fuel. Although a significant number of MOX fuel rods have been tested in Cabri and NSRR, REP-Na7 is the only such test that produced cladding failure. From the raw data, we see no systematic difference in failure (or non-failure) enthalpies. Because failure is dominated by cladding properties, the fuel type inside would only affect the applied loading. Because the dominant loading is simple thermal expansion of the pellet, it is unlikely that different fuel types (MOX or gadolinia) would affect this very much.[c]

The FRAPTRAN code, which we use for analysis, does not contain MOX fuel properties at the present time. The NRC steady-state code, FRAPCON, does contain MOX fuel properties, so these properties have been studied and have only a modest effect on code output. Nevertheless, this difference is probably unimportant for the FRAPTRAN analysis done here. This is because we back out of the analysis the strain that would cause the observed failure and then calculate the effect of temperature changes on the enthalpy that would produce this

[c]It is likely, however, that inhomogenieties in MOX fuel would affect fuel pellet breakup and dispersal of fuel particles in the case of cladding failure.

strain. If the strain value is off by a modest amount due to MOX properties, the calculated enthalpy change would hardly be affected.

This test was analyzed by examining the failure strain in the plastic region, as discussed in Section 5.3. Using FRAPTRAN, plastic strain and other parameters were calculated as a function of time for the actual test reactor pulse. Calculated parameters at the reported time of failure for REP-Na7 are shown in Table 17.

Table 17 Calculated Parameters for REP-Na7	
Effective Gap (Input)	95 μ
Cladding Plastic Strain = Failure Strain	0.49 %
Cladding Average Temperature	720°C
Fuel Enthalpy Change at Failure	97 cal/g

The calculated value of plastic strain is not in very good agreement with the measured values from Cabri in Fig. 14, but the calculated enthalpy change at failure is in good agreement with the value reported by the French investigators (97 cal/g; see Table 3 and subtract 16 cal/g from their calculated enthalpy at failure to correct for the initial test temperature).

A second calculation was run with the same 172 cal/g deposited energy, but with a pulse shape and other input corresponding to PWR conditions. Power traces for the REP-Na7 test pulse and the PWR-shaped pulse with the same deposited energy are shown in Fig. 18. Using the

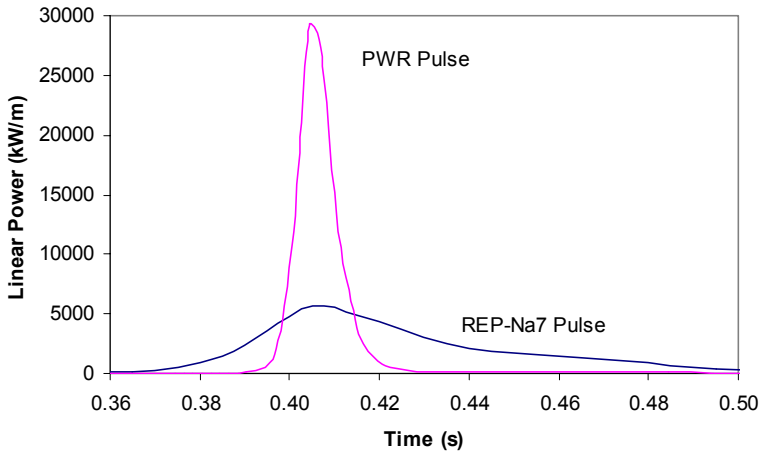

Figure 18. Power versus time for the broad REP-Na10 test pulse and a PWR-shaped pulse with the same deposited energy.

method described in Sections 5.1 and 5.3, cladding failure should occur for this specimen when the calculated plastic strain in the second calculation reaches 0.49%; no change in uniform elongation, total elongation, or failure strain was made because the Cabri test was run at the

PWR accident temperature. This plastic strain occurs at 73 cal/g in the second calculation, and this is 24 cal/g lower than the enthalpy at failure in the first calculation (97 - 73 = 24). The decrease results from the fact that a much larger portion of the total strain (related to enthalpy) is elastic strain at the lower temperature in the second calculation (see Section 5.4).

However, higher strain values were calculated at later times in the second calculation. Because we are ultimately interested in a cladding failure threshold, a pulse is desired that has the minimum deposited energy that will result in a peak plastic strain of 0.49%. The energy deposited in the second calculation is obviously too high.

Additional calculations were performed to search for the smallest pulse that would reach 0.49% plastic strain. The results for this threshold pulse are given in Table 18.

Table 18 Calculated Parameters for a Threshold Pulse with the REP-Na7 Specimen under PWR Conditions	
Inlet Coolant Temperature (Input)	280°C
Total Energy Deposited (Input)	84 cal/g
Pulse Width (FWHM, Input)	12 ms
Effective Gap (Input)	95 μ
Peak Cladding Plastic Strain = Failure Strain	0.49 %
Cladding Average Temperature at Failure	640°C
Maximum Fuel Enthalpy Change	78 cal/g

This calculation has produced a slightly different result. The peak fuel enthalpy that will generate the failure strain of 0.49% is 19 cal/g lower than the failure enthalpy observed in the test, rather than 24 cal/g lower as found in the second calculation. Essentially all of this difference is due to the rate effects discussed above.

6.4. NSRR HBO-1 (failure in the plastic region)

Measured test parameters for HBO-1 are shown in Table 19.

Table 19 Measured Parameters for HBO-1	
Initial Coolant Temperature	18°C
Total Energy Deposited	93 cal/g
Pulse Width (Full Width at Half Maximum, FWHM)	4.4 ms
Time of Peak Power	0.2023 s
Time of Failure	0.2040 s

This test was analyzed by examining the failure strain in the plastic region, as discussed in Section 5.3. Using FRAPTRAN, plastic strain and other parameters were calculated as a function of time for the actual test reactor pulse. Calculated parameters at the reported time of failure for HBO-1 are shown in Table 20.

Table 20 Calculated Parameters for HBO-1	
Effective Gap (Input)	10 μ
Cladding Plastic Strain = Failure Strain	0.52 %
Cladding Average Temperature	65°C
Fuel Enthalpy Change at Failure	57 cal/g

The calculated value of plastic strain is in good agreement with the measured values for the HBO series in Fig. 14, and the calculated enthalpy change at failure is in good agreement with the calculated value reported by the Japanese investigators (60 cal/g; see Table 4).

A second calculation was run with the same 93 cal/g deposited energy, but with a pulse shape and other input corresponding to PWR conditions, including a 95 micron gap. Power traces for the HBO-1 test pulse and the PWR-shaped pulse with the same deposited energy are shown in Fig. 19. The peak plastic strain developed in this calculation was only 0.261%, so power had to be increased in additional calculations to reach a failure strain.

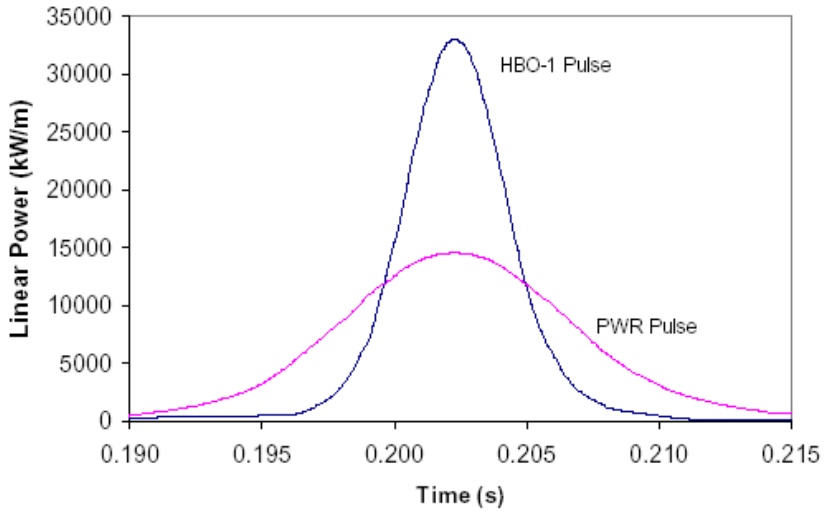

Figure 19. Power versus time for the broad HBO-1 test pulse and a PWR-shaped pulse with the same deposited energy.

Two different failure strains were used as discussed in Section 5.3. One failure strain assumed the temperature dependence of the cladding's uniform elongation. Because no temperature dependence of uniform elongation was seen (Fig. 11) in the temperature range from 18°C

(NSRR test temperature) to 280°C (hot-zero-power PWR temperature), the first failure strain was the same as that found for the test pulse, namely 0.52%. The other failure strain assumed the temperature dependence of the cladding's total elongation. Using the linear correlation in Fig. 12, the 0.52% value was increased by the ratio of total elongation at 277°C to that at 18°C. This gave a failure strain of 2.48%

Additional calculations were performed to search for the smallest pulses that would reach 0.52% and 2.48% plastic strains, respectively. The results for these threshold pulses are given in Table 21, and the two cases are identified by the letters UE and TE.[d]

Table 21 Calculated Parameters for two Threshold Pulses with the HBO-1 Specimen under PWR Conditions

Inlet Coolant Temperature (Input)	277°C
Total Energy Deposited (Input)	109 cal/g (UE) 195 cal/g (TE)
Pulse Width (FWHM, Input)	10 ms
Effective Gap (Input)	95 μ
Peak Cladding Plastic Strain = Failure Strain	0.52% (UE) 2.48% (TE)
Cladding Average Temperature at Failure	670°C (UE) 829°C (TE)
Maximum Fuel Enthalpy Change	80 cal/g (UE) 142 cal/g (TE)

These calculations show that a significantly higher enthalpy change than that found in the test would be expected to achieve cladding failure with the HBO-1 specimen if it had experienced a rod ejection accident in a PWR. Because the appropriate temperature dependence is not known, this correction could be between 23 cal/g and 74 cal/g above the test result of 57 cal/g. This large correction is thus much more uncertain than the small corrections made for the Cabri tests.

6.5. NSRR TK-2 (failure in the plastic region)

Measured test parameters for TK-2 are shown in Table 22.

[d]Local fuel melting was observed in the TE calculation in the next-to-outer nodal ring at a radially averaged enthalpy of 119 cal/g. Local melting at this relatively low energy was predicted because of the very high edge peaking of the power in high-burnup fuel; melting would occur at a higher enthalpy in low-burnup fuel.

Table 22 Measured Parameters for TK-2	
Initial Coolant Temperature	25°C
Total Energy Deposited	136 cal/g
Pulse Width (Full Width at Half Maximum, FWHM)	4.4 ms
Time of Peak Power	0.2073 s
Time of Failure	0.2077 s

This test was analyzed by examining the failure strain in the plastic region, as discussed in Section 5.3. Using FRAPTRAN, plastic strain and other parameters were calculated as a function of time for the actual test reactor pulse. Calculated parameters at the reported time of failure for TK-2 are shown in Table 23.

Table 23 Calculated Parameters for TK-2	
Effective Gap (Input)	10 μ
Cladding Plastic Strain = Failure Strain	0.58 %
Cladding Average Temperature	58°C
Fuel Enthalpy Change at Failure	59 cal/g

The calculated value of plastic strain is again in good agreement with the measured values for the HBO and TK series in Fig. 14, and the calculated enthalpy change at failure is in good agreement with the calculated value reported by the Japanese investigators (60 cal/g; see Table 4).

A second calculation was run with the same 136 cal/g deposited energy, but with a pulse shape and other input corresponding to PWR conditions, including a 95 micron gap. Power traces for the TK-2 test pulse and the PWR-shaped pulse with the same deposited energy are shown in Fig. 20. The peak plastic strain developed in this calculation was 0.815%, so the power had to be increased in one case and decreased in the other case to reach the desired threshold values.

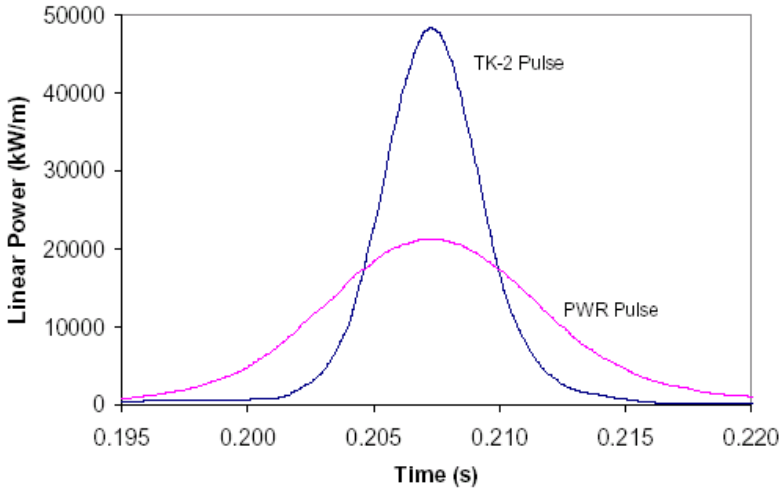

Figure 20. Power versus time for the broad TK-2 test pulse and a PWR-shaped pulse with the same deposited energy.

Two different failure strains were used in the manner discussed in Section 5.3. One failure strain assumed the temperature dependence of the cladding's uniform elongation. Because no temperature dependence of uniform elongation was seen (Fig. 11) in the temperature range from 18°C (NSRR test temperature) to 280°C (hot-zero-power PWR temperature), the first failure strain was the same as that found for the test pulse, namely 0.58%. The other failure strain assumed the temperature dependence of the cladding's total elongation. Using the linear correlation in Fig. 12, the 0.58% value was increased by the ratio of total elongation at 277°C to that at 18°C. This gave a failure strain of 2.54%

Additional calculations were performed to search for the smallest pulses that would reach 0.58% and 2.54% plastic strains, respectively. The results for these threshold pulses are given in Table 24, and the two cases are identified by the letters UE and TE.[e] These calculations show that a significantly higher enthalpy change than that found in the test would be expected to achieve cladding failure with the TK-2 specimen if it had experienced a rod ejection accident in a PWR. Because the appropriate temperature dependence is not known, this correction could be between 27 cal/g and 71 cal/g above the test result of 59 cal/g. This large correction is consistent with that found for HBO-1 and is much more uncertain than the small corrections made for the Cabri tests.

[e]Local fuel melting was also observed in this (TE) calculation in the next-to-outer nodal ring at a radially averaged enthalpy of 112 cal/g.

Table 24 Calculated Parameters for two Threshold Pulses with the TK-2 Specimen under PWR Conditions	
Inlet Coolant Temperature (Input)	277°C
Total Energy Deposited (Input)	117 cal/g (UE) 175 cal/g (TE)
Pulse Width (FWHM, Input)	11 ms (UE) 6 ms (TE)
Effective Gap (Input)	95 μ
Peak Cladding Plastic Strain = Failure Strain	0.58% (UE) 2.54% (TE)
Cladding Average Temperature at Failure	655°C (UE) 735°C (TE)
Maximum Fuel Enthalpy Change	86 cal/g (UE) 130 cal/g (TE)

7. Cladding Failure Thresholds

Results from these calculations can be employed to get an estimate of cladding failure thresholds from the test-reactor failure data in Fig. 3. First, however, a further observation can be made about the two NSRR tests (HBO-1 and TK-2) that were analyzed and scaled for PWR conditions. A wide range was found for the scaling correction because it is not known whether to use the temperature dependence of measured uniform elongation values or total elongation values. Several factors argue for choosing the temperature dependence of uniform elongation.

Above all, appropriate assumptions in the analysis should lead to improved consistency between NSRR and Cabri data. Choosing the uniform temperature dependence (i.e., no temperature variation between room temperature and 300°C) produces this result. The scaled enthalpy changes at failure for REP-Na7, HBO-1, and TK-2, which all had similar oxide thicknesses, are 78, 80, and 86 cal/g, respectively. These are very consistent results compared with either the unadjusted results or the results adjusted with the temperature dependence of total elongation.

This choice also produces a conservative result, such that any errors in this choice should not make the result non-conservative. Further, FRAPTRAN and most other codes calculate uniform deformation and are not able to calculate necking and other localized phenomena; therefore, this is the most logical choice for the analysis. And a benefit of this choice is that the absence of any pronounced temperature variation of uniform elongation in this temperature range is the best understood area of the plastic properties.

Using this choice, adjustments for HBO-1 and TK-2 are +23 cal/g and +27 cal/g, respectively. For plotting purposes, all NSRR failure points have thus been adjusted to hot zero-power PWR conditions by adding 25 cal/g. The three Cabri failure points have been plotted as they were individually adjusted in our calculations. The Russian IGR and BIGR test data produced non-PCMI failures and have been plotted without adjustment. The PBF data were obtained with approximately the right pulse width and test temperature, and therefore were not adjusted. The SPERT data were obtained with approximately the right pulse width, but with the wrong test temperature; however, the completeness of the data for these old tests did not make scaling practical. Figure 21 shows the data after these adjustments have been made. A PWR cladding failure threshold, which is used in Section 8, is also drawn on the figure. The following considerations were used in selecting this threshold.

One prominent data point has been ignored (14 cal/g at 80 microns). This point is for Cabri's REP-Na1 test, which was discussed in Section 2.3. The 150 cal/g intercept is consistent with the traditional 170 cal/g total enthalpy value when 16 cal/g are subtracted for the 280°C hot zero power temperature to get an enthalpy change. Although the technical basis for the traditional 170 cal/g value appears to have been lost, that value is consistent with the IGR and BIGR test results in which failure occurred by a swelling and rupture (not PCMI).

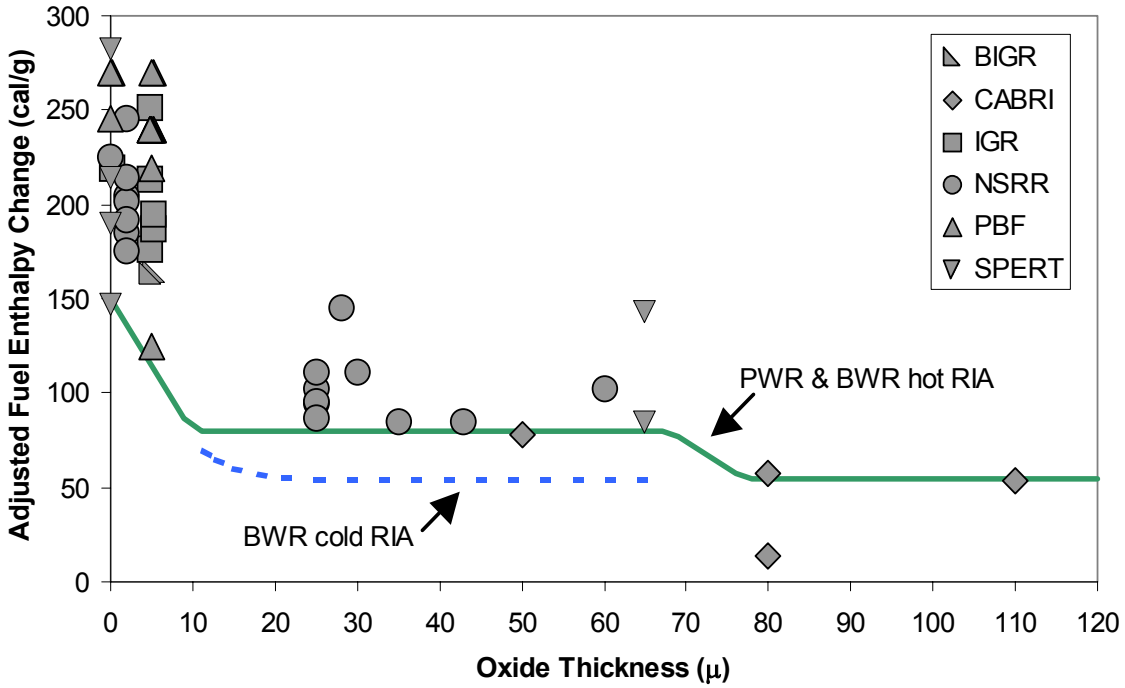

Figure 21. Cladding failure data with adjustments from the scaling analysis and lower-bound failure correlations.

A corrosion thickness of 10 microns corresponds to approximately 100 ppm of hydrogen. More than half of this hydrogen will be in solution under PWR-relevant RIA conditions. The remaining amount (less than 50 ppm) will be precipitated as sparsely-distributed circumferential hydrides, which are considered to be benign with regard to failure limits. Therefore, a substantial reduction in the failure threshold due to hydrogen embrittlement should not occur below 10 microns. This picture agrees with the data.

The remainder of the correlation line is drawn to provide a lower bound to the adjusted PCMI failure points from Cabri and NSRR. Much of the remaining scatter in these data is stochastic in nature and probably due to the presence of fuel fines and chips in pellet cracks and gaps; therefore, a bounding correlation is appropriate.

The SPERT CDC-859 data point is not as well documented as the others; nevertheless, it is thought that the specimen had about 65 microns of oxide and exhibited significant plastic strain. Therefore, based on this point, the downward trend toward substantially brittle failure was initiated after 65 microns.

The PWR failure threshold in Fig. 21 is also appropriate for BWR RIAs that initiate from hot conditions because BWR rods are included in the database. For cold zero-power rod drop accidents, however, the threshold should correspond to the unadjusted NSRR data because those data were taken under cold conditions. This threshold is also shown in Fig. 21. Zircaloy-2 under BWR conditions does not accumulate corrosion above 65 microns, so the BWR (cold) threshold is not continued above that level.

Notice that the database represented by the thresholds in Fig. 21 contains a wide manufacturing variety of Zircaloy-2 and Zircaloy-4 cladding, as well as MDA, E110, Zirlo, and M5 cladding alloys. This latter group of alloys tends to oxidize less than Zircaloy-4, and their corrosion resistance is accounted for by correlating the failure enthalpy with oxide thickness (rather than burnup). Testing with Zirlo and M5 has been very limited to date. It can be noted, however, that Cabri CIP0-1 (Zirlo) provides interesting corroboration. That test had 80 microns of oxide, experienced a 32 ms pulse, reached a peak fuel enthalpy of 90 cal/g and did not fail. This can be compared with REP-Na10 (Zircaloy-4), which had 80 microns of oxide, experienced a 31 ms pulse, reached a peak fuel enthalpy of 98 cal/g and failed. CIP0-1 would fall about 5 cal/g below the failure threshold in Fig. 21 if this test had been analyzed (based on similarities to the REP-Na10 analysis).

It should also be noticed that the database contains a number of MOX fuel rods. A MOX rod, REP-Na7, was one of the tests that was analyzed. Although inhomogenieties in MOX fuel might affect the propensity for fuel dispersal (given a cladding failure), there is no reason to believe that MOX would significantly affect the cladding failure threshold, which is driven by thermal expansion (thermal properties of MOX and UO_2 are quite similar). Therefore, the failure thresholds in Fig. 21 should also be applicable to MOX fuel.

8. Fuel Enthalpy Limits

The original 280 cal/g fuel enthalpy limit – and even the 230 cal/g limit that MacDonald suggested – were well above the threshold for cladding failure. Nevertheless, a limit at this level was sufficient to prevent fuel dispersal from fresh or very low burnup fuel; fuel melting was needed to eject fuel from a defected fuel rod, and fuel melting required high enthalpy levels. Hence, two separate values were used in typical safety analyses: the 280 (or 230) limit to ensure against fuel dispersal and its consequences, and some lower threshold value to indicate the occurrence of cladding failure for radiological calculations. This two-value approach was adequate because neither the generation of pressure pulses nor the loss of coolable fuel geometry could occur without fuel dispersal.

For high-burnup fuel, another mechanism is present to disperse fuel; namely, the rapid expansion of fission gas bubbles that reside on grain boundaries. Fuel dispersal is seen in many tests that have just enough energy to cause cladding failure by PCMI.

General Design Criterion 28 does not necessarily require the containment of all fuel particles within fuel rod cladding. It only requires that the amount and rate of reactivity increase for RIAs neither damage the reactor coolant pressure boundary nor significantly impair core coolability. If fuel dispersal is permitted, however, two questions arise that are difficult to answer. Will the pressure pulses generated by the prompt dispersal of hot fuel particles into water be small enough that they will not damage the reactor pressure boundary? Will dispersed fuel particles be coolable? In this assessment, we have chosen not to attempt to answer these questions. Therefore, the cladding failure threshold has been used as the fuel enthalpy limit. Without cladding failure, there can be no fuel dispersal, no damaging pressure pulses, and no loss of coolable geometry.

For low-burnup fuel, a two-value approach could be used because fuel dispersal would not be concomitant with cladding failure. However, we have not examined the database to determine if a burnup level could be found where there is insufficient fission gas to cause grain boundary separation. This, of course, would make the assessment of operating reactors more complicated, and this complication was not necessary to complete the assessment. Consequently, for all cases in this assessment, the cladding failure thresholds in Fig. 21 have been used as the fuel enthalpy limits.

9. Control Rod Worth

To complete the assessment of postulated reactivity accidents in PWRs and BWRs, plant analyses had been performed to examine the conditions necessary to reach the cladding failure thresholds in Fig. 21. Most attention has been given to the PWR rod-ejection accident, and that analysis will be discussed first.[30]

The analysis was done with a model of the TMI-1 reactor with the PARCS 3-dimensional neutron kinetics code. Reactor conditions were considered at both end-of-cycle and beginning-of-cycle. In order to consider different control rod worths, neutron cross sections were modified for the central fuel assembly, which was the location of the ejected rod.[f] The control rod was ejected in 100 ms from hot zero power conditions and reactor trip was initiated when power reached 112% of full power. In addition to varying control rod worth, the delayed neutron fraction at end-of-cycle was varied from 70 to 120% of the nominal value. For each transient simulation of a given rod worth and delayed neutron fraction, there was a maximum change in fuel pellet enthalpy considering all mesh points in the model.

The variation of the maximum enthalpy change with rod worth normalized by the delayed neutron fraction (i.e., in units of dollars), is given in Figure 22. The dependence of fuel

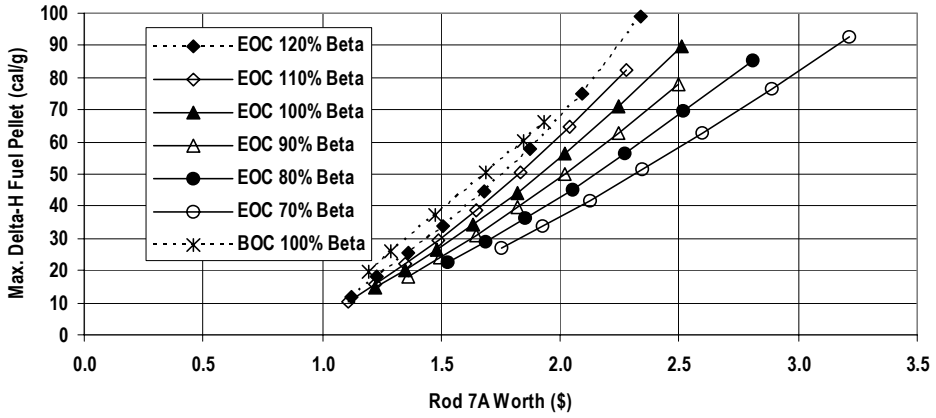

Figure 22. Maximum fuel enthalpy change for a PWR rod ejection accident from hot zero power as a function of control rod worth for various values of delayed-neutron fraction (beta).

enthalpy with rod worth is approximately linear, and it increases with the delayed neutron fraction. As the value of the delayed neutron fraction at end-of-cycle approaches that at beginning-of-cycle, so too does the enthalpy change in the figure. For example, the enthalpy change for a $1.5 rod ejection accident is approximately 26 cal/g for end-of-cycle (beta = 0.005211), 34 cal/g for end-of-cycle with 120% beta (0.006253), and 37 cal/g for beginning-of-cycle (beta = 0.006323). For rod ejection accidents with rod worths below $1.5, the enthalpy

[f]An alternative method in which fuel assemblies were shuffled to increase control rod worth yielded similar results.

rise is less than 40 cal/g. To get an enthalpy rise above 100 cal/g requires an rod ejection accident of more than $2.3 for the conditions assumed in these studies.

The variation of the maximum enthalpy change as a function of the difference between the rod worth and the delayed neutron fraction is given in Figure 23. All the data points at end-of-cycle

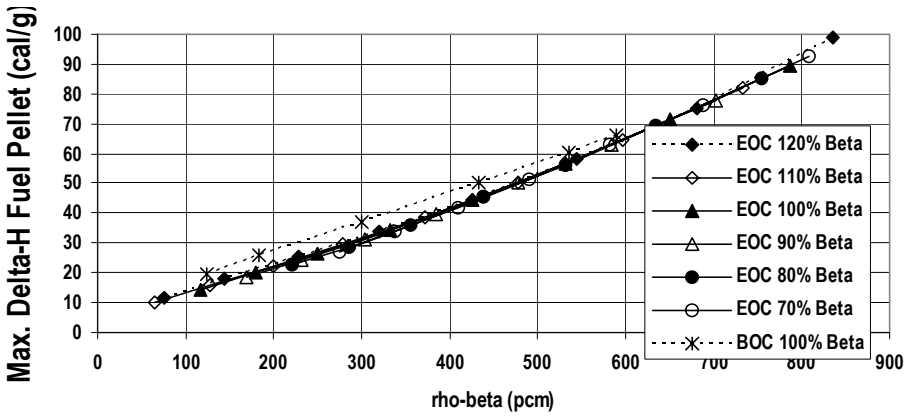

Figure 23. Maximum fuel enthalpy change for a PWR rod ejection accident from hot zero power as a function of the difference between control rod worth (rho) and delayed-neutron fraction (beta).

for various rod worths and delayed neutron fractions collapse onto a single (almost) linear curve. Hence, the absolute difference between the ejected rod worth and the delayed neutron fraction, the absolute reactivity above prompt critical, determines the maximum fuel pellet enthalpy change, with all other quantities fixed. The curve for the beginning-of-cycle case is set about 5 to 10 cal/g higher than most of the curves for end-of-cycle at any given rod worth exceeding the delayed neutron fraction. The higher enthalpy change for the beginning-of-cycle case can be explained by the presence of lower burnup assemblies at beginning-of-cycle. Lower burnup assemblies will experience a higher fission rate and power increase for a given control rod worth during a rod ejection accident.

The results show that the enthalpy change is less than 70 cal/g for rod worths less than $2. This is an extremely high control rod worth. In most PWRs, normal rod worths are less than $1. However, in some situations with distorted spatial xenon distributions or in some reactors with control rods at positions of fresh fuel, the worth can be greater than $1. There is no comprehensive database of rod worths in U.S. power reactors. Based on available data, however, it is very unlikely for a rod worth to exceed $1.5.[37] At this value, the enthalpy change is only 40 cal/g at beginning-of-cycle.

This 40 cal/g fuel enthalpy change can be compared with the PWR cladding failure threshold in Fig. 21. The enthalpy change falls below the failure threshold, even for heavily corroded cladding above about 70 microns of oxide thickness. Hence, the conclusion is that fuel dispersal would not take place should an RIA occur in an operating PWR.

A similar conclusion can be reached for BWRs without performing specific analyses. Our calculations for BWRs generally result in lower values of fuel enthalpy change than for PWRs, so there would still be some margin to the BWR cold failure threshold. The broader pulse widths in BWRs may also have less of a tendency to disperse fuel when there is a cladding failure. Also, the probability of a BWR rod drop accident is significantly lower than the probability of a PWR rod ejection accident.[7] Taken together, these factors indicate that it would be very unlikely to get cladding failure during a BWR rod drop accident, thus ensuring coolable geometry and precluding steam explosions.

10. Summary and Conclusions

The current fuel enthalpy limit used in safety analyses for reactivity-initiated accidents (RIAs) is 280 cal/g, based on early tests with low-burnup and unirradiated fuel rods. That limit was intended to preclude fuel dispersal by avoiding incipient melting of UO_2. By precluding fuel dispersal, a coolable fuel geometry was ensured and steam explosions could not occur.

High-burnup fuel behaves differently. In late 1993 and early 1994, tests in France and Japan showed that cladding failure with fuel dispersal could occur at fuel enthalpies below 100 cal/g. Since that time, tests in France, Japan, and Russia have confirmed this high-burnup behavior and generated a database that permits an updated assessment of postulated RIAs for operating reactors.

The test reactors in which the data were developed, however, did not reproduce LWR conditions well, and the atypicalities are believed to have biased some of the results. An estimate of this bias was therefore desired. Using NRC's FRAPTRAN fuel rod code, a method has been developed to perform a scaling analysis to adjust raw test data for LWR conditions, and the method has been used to adjust some of the most influential test results in the database. The adjustments range only from -17 cal/g to +27 cal/g, so the final result is still largely empirical and closely related to the measured data. From these adjusted results, RIA cladding failure thresholds have been estimated for PWR and BWR fuels. The adjusted data and the thresholds are shown in Fig. 21. These thresholds apply to Zircaloy-2, Zircaloy-4, Zirlo, and M5 cladding alloys as well as to UO_2 and MOX fuel, all of which were included in the database.

In high-burnup fuel, expanding fission gas is able to drive fuel particles out through a cladding breach whereas fuel melting was needed as the driving force in low-burnup fuel. Thus, many — if not most — cladding failures in high-burnup fuel might be accompanied by fuel dispersal. Consequently, the cladding failure thresholds were used as the enthalpy limits for this assessment, rather than using a higher limit based on fuel melting.

Neutronic analyses were then performed for a range of LWR conditions, and it was found that control rod worths needed to reach the enthalpy limits were very high (above $1.5). There is no comprehensive database of rod worths in U.S. power reactors. Based on available data, however, it is very unlikely for a rod worth to exceed $1.5. Therefore, it was concluded that current operating reactors are not likely to experience cladding failure during the worst postulated RIAs. Without cladding failure, coolable geometry is ensured and steam explosions cannot occur.

It should be noted that cladding failure thresholds vary only weakly with burnup level. Cladding corrosion (oxidation), which might differ widely for different cladding materials at the same burnup, was found to be the most important variable. The cladding failure thresholds (hence enthalpy limits) in this assessment were developed in terms of oxide thickness, rather than burnup, and were therefore directly applicable to different cladding materials.

11. References

1. P. E. MacDonald, S. L. Seiffert, Z. R. Martinson, R. K. McCardell, D. E. Owen, and S. K. Fukuda, "Assessment of Light-Water-Reactor Fuel Damage During a Reactivity-Initiated Accident," *Nuclear Safety* 21, September-October 1980, pp. 582-602.

2. R. O. Meyer, D. A. Powers, M. Tokar, and J. C. Voglewede, "Licensing Requirements for Fuel Behavior During DBAs," *Proceedings ANS Topical Meeting: Reactor Safety Aspects of Fuel Behavior*, Sun Valley 1981, pp. 2/92-2/99.

3. F. Schmitz, J. Papin, M. Haessler, J. Nervi, and P. Permezel, "Investigation of the behaviour of high-burnup PWR fuel under RIA conditions in the CABRI test reactor," *Proceedings 22nd WRSM*, NUREG/CP-0140 Vol. 2, April 1995, pp. 329-349.

4. T. Fuketa, Y. Mori, H. Sasajima, K. Ishijima, and T. Fujishiro, "Behavior of High Burnup PWR Fuel Under a Simulated RIA Condition in the NSRR," *Specialist Meeting on Transient Behaviour of High Burnup Fuel*, September 12-14, 1995, Cadarache, NEA/CSNI/R(95)22, 1996, pp. 59-85.

5. H. Rosenbaum, R. Montgomery, V. Bessiron, J. Desquines, and H. Chung, "Resolving our Understanding of REP-Na1," EPRI report to be published.

6. R. O. Meyer, R. K. McCardell, H. M. Chung, D. J. Diamond, and H. H. Scott, "A Regulatory Assessment of Test Data for Reactivity-Initiated Accidents, *Nuclear Safety* 37, October-December 1996, pp. 271-288.

7. L. J. Callan, "Agency Program Plan for High-Burnup Fuel," memorandum to the Commission, July 6, 1998.

8. W. D. Travers, "Updated Program Plan for High-Burnup Light-Water Reactor Fuel," memorandum to the Commission, August 21, 2003.

9. R. W. Miller, "The Effects of Burnup on Fuel Failure, Power Burst Tests on Fuel Rods with 13,000 and 32,000 MWd/MTU Burnup," ANCR-1280, January 1976.

10. B. A. Cook and Z. R. Martinson, "Reactivity Initiated Accident Test Series, Test RIA 1-4 Fuel Behavior Report," NUREG/CR-3938, September 1984.

11. S. L. Seiffert, Z. R. Martinson, and S. K. Fukuda, "Reactivity Initiated Accident Test Series, Test RIA-1-1 (Radial Average Fuel Enthalpy of 285 cal/g) Fuel Behavior Report," NUREG/CR-1465, September 1980.

12. R. S. Semken, S. Shiozawa, Z. R. Martinson, R. K. McCardell, P. E. MacDonald, J. A. Fernandez, and S. K. Fukuda, "Reactivity Initiated Accident Test Series, RIA Scoping Tests Fuel Behavior Report," NUREG/CR-1360, April 1980.

13. B. A. Cook, S. K. Fukuda, Z. R. Martinson, and P. Bott-Hembree, "Reactivity Initiated Accident Test Series, Test RIA 1-2 Fuel Behavior Report, NUREG/CR-1842, January 1981.

14. J. Papin, B. Cazalis, J.M. Frizonnet, E. Fédérici, F. Lemoine," Synthesis of Cabri-ria Tests Interpretation," Eurosafe Conference, November 2003, Paris.

15. IRSN Press Release, "IRSN completes first test in its international Cabri-Water Loop research program," www.irsn.fr, release 14/11/2002.

16. IRSN Press Release, "IRSN performs the second test of the Cabri-Water Loop international research program," www.irsn.fr, release 04/12/2002.

17. T. Fujishiro, K. Yanagisawa, K. Ishijima, and K. Shiba, "Transient Fuel Behavior of Preirradiated PWR Fuels Under Reactivity Initiated Accident Conditions," *J. Nuclear Materials,* Vol. 188, 1992, pp. 162-167.

18. T. Nakamura, M. Yoshinaga, M. Sobajima, K. Ishijima, and T. Fujishiro, "Boiling Water Reactor Fuel Behavior at Burnup of 26 GWd/tonne U under Reactivity-Initiated Accident Conditions, *Nuclear Technology*, Vol. 108, 1994, pp. 45-60.

19. T. Fuketa, F. Nagase, K. Ishijima, and T. Fujishiro, "NSRR/RIA Experiments with High-Burnup PWR Fuels", *Nuclear Safety*, Vol.37, No.4, 1996, pp.328-342.

20. T. Fuketa, H. Sasajima, and T. Sugiyama, "Behavior of High-Burnup PWR Fuels with Low-Tin Zircaloy-4 Cladding Under Reactivity-Initiated-Accident Conditions," *Nuclear Technology*, Volume 133 Number 1, January 2001, pp. 50-62.

21. T. Fuketa, H. Sasajima, Y. Mori, and K. Ishijima, "Fuel Failure and Fission Gas Release in High Burnup PWR Fuels under RIA Conditions", *J. Nuclear Materials*, Vol.248, 1997, pp.249-256.

22. T. Nakamura et al., "NSRR RIA Tests Results and Experimental Programmes," *Proceedings of the Topical Meeting on RIA Fuel Safety Criteria*, Aix-en-Provence, France, 13-15 May 2002 (NEA/CSNI/R(2003)8/Vol. 2) pp. 83-95.

23. T. Nakamura, K. Kusagaya, T. Fuketa, and H. Uetsuka, "High-Burnup BWR Fuel Behavior Under Simulated Reactivity-Initiated Accident Conditions," *Nuclear Technology*, Volume 138 Number 3, June 2002, pp. 246-259.

24. V. Asmolov and L. Yegorova, "Development and Performance of Research Programme for Analysis of High Burn-up Fuel Rod Behavior under RIA Condition at IGR Pulse Reactor," *OECD Specialist Meeting on Transient Behavior of High Burnup Fuel*, September 12-14, 1995, Cadarache, NEA/CSNI/R(95)22, 1996, pp. 155-165.

25. G. Abyshov et al., "Data Base on The Behavior of High Burnup Fuel Rods With Zr-1%Nb Cladding and UO2 Fuel (VVER Type) Under Reactivity Accident Conditions," NUREG/IA-0156, July 1999.

26. V. Asmolov and L. Yegorova, "Recent Results on the RIA Test in IGR Reactor," *Proceedings 24th WRSM*, NUREG/CP-0157, January 1997, pp. 131-139.

27. Y. Bibilashvili et al., “Study of High Burnup VVER Fuel Rods Behaviour at the BIGR Reactor Under RIA Conditions: Experimental Results,” *Proceedings of the Topical Meeting on RIA Fuel Safety Criteria*, Aix-en-Provence, France, 13-15 May 2002 (NEA/CSNI/R(2003)8/Vol. 2) pp. 115-129.

28. G. Berna, C. Beyer, K. Davis, and D. Lanning, “FRAPCON-3: A Computer Code for the Calculation of Steady-State, Thermal-Mechanical Behavior of Oxide Fuel Rods for High Burnup,” NUREG/CR-6534 vol 2, December 1997.

29. J. Lewins, “The adiabatic Fuchs-Nordheim model and non-dimensional solutions,” *Ann. Nuclear Energy*, Vol. 22 No. 10, October 1995, pp. 681-686.

30. D.J. Diamond, B.P. Bromley, and A.L. Aronson, “Studies of the Rod Ejection Accident in a PWR,” Technical Report W6382, Brookhaven National Laboratory, January 22, 2002.

31. P. H. Kreyns et al., “Embrittlement of Reactor Core Materials,” *Zirconium in the Nuclear Industry: Eleventh International Symposium*, ASTM STP 1295, E. Bradley and G. Sabol, Eds., American Society for Testing and Materials, 1996, pp. 758-782.

32. K. Edsinger, J. Davis, and R. Adamson, “Degraded Fuel Cladding Fractography and Fracture Behavior,” *Zirconium in the Nuclear Industry: Twelfth International Symposium*, ASTM STP 1354, G. Sabol and G. Moan, Eds., American Society for Testing and Materials, 2000, pp. 316-339.

33. M. E. Cunningham, C. E. Beyer, P. G. Medvedev and G. A. Berna, FRAPTRAN: A Computer Code for the Transient Analysis of Oxide Fuel Rods, U.S. Nuclear Regulatory Commission Report NUREG/CR-6739 (PNNL-13576), August 2001.

34. M. Balourdet, C. Bernaudat, V. Basini, and N. Hourdequin, "The PROMETRA Programme : assessment of mechanical properties of zircaloy-4 cladding during an RIA", *SMIRT 15,* Vol.II, 1999, pp. 485-492.

35. K. Geelhood, C. Beyer, and M. Cunningham, “Modifications to FRAPTRAN to Predict Fuel Rod Failures Due to PCMI,” 2004 International Meeting on LWR Fuel Performance, ANS to be published.

36. J. Desquines et al., “Zircaloy-4 Fuel Cladding Mechanical Behavior in the Field of RIA Transients through the PROMETRA Program, *Zirconium in the Nuclear Industry*, (Stockholm 2004), ASTM to be published.

37. Y. A. Chao, D. M. Chapman, D. J. Hill, and L. R. Grobmyer, “Dynamic Rod Worth Measurement,” *Nuclear Technology* 132, December 2000, pp. 403-412.